

CZECH UNIVERSITY OF LIFE SCIENCES PRAGUE

Faculty of Environmental sciences

**DEPARTMENT OF WATER RESOURCES AND ENVIRONMENTAL
MODELING - FES**



**REKONSTRUKCE NĚMECKÝCH LETNÍCH POVODNÍ 2021
POMOCÍ „DATA-DRIVEN” METOD
RECONSTRUCTING THE GERMAN SUMMER FLOODS 2021
USING THE DATA-DRIVEN METHODS**

BACHELORE THESIS

Supervisor: **Ing. Oldřich Rakovec, Ph.D.**

Student: **Ronak Rahmati**

2023

BACHELOR THESIS ASSIGNMENT

Ronak Rahmati

Environmental Data Science
Informatics

Thesis title

Reconstructing of the German summer floods 2021 using the data-driven methods

Objectives of thesis

Aim: This study aims to explore the ability of data-driven methods to reconstruct the flooding magnitude of the devastating summer 2021 floods in the Ahr River basin (Germany). The effect of the meteorological uncertainty will be analysed as well.

Methodology

Tasks/methods:

1. Get familiar with the data-driven methods (LSTM or BRNN) available in R.
2. Prepare the time series meteorological forcing data for the Ahr River based on the global data: ERA5-land, ERA5, continental data: EOBS, German-based data: Regnie.
3. Analyse the differences in the rainfall estimates (long-term statistics and summer 2021).
4. Calibrate/train the LSTM and BRNN models against daily river flows (1981-2020) using spatially lumped and distributed forcing data.
5. Evaluate the performance of the models during the training period (2021, with a particular focus on July 2021): compare LSTM & BRNN against different meteorological data.
6. Assess the effect of the initial conditions on the flood peak

The proposed extent of the thesis

30 pages + figures + model code

Keywords

data driven model, floods, initial conditions, meteorologic uncertainty

Recommended information sources

- Abadi, M., Barham, P., Chen, J., Chen, Z., Davis, A., Dean, J., Devin, M., Ghemawat, S., Irving, G., Isard, M., et al.: Tensorflow: A system for large-scale machine learning, in: 12th USENIX symposium on operating systems design and implementation (OSDI 16), pp. 265–283, 2016.
- Arnold, T. B.: kerasR: R interface to the keras deep learning library, *Journal of Open Source Software*, 2, 296, 2017.
- Kratzert, F., Klotz, D., Shalev, G., Klambauer, G., Hochreiter, S., and Nearing, G.: Towards learning universal, regional, and local hydrological behaviors via machine learning applied to large-sample datasets, *Hydrol. Earth Syst. Sci.*, 23, 5089–5110, <https://doi.org/10.5194/hess-23-5089-2019>, 2019.
- Kreienkamp, F., Philip, S.Y., Tradowsky, J.S., Kew, S.F., Lorenz, P., Arrighi, J., Belleflamme, A., Bettmann, T., Caluwaerts, S., Chan, S.C. and Ciavarella, A., 2021. Rapid attribution of heavy rainfall events leading to the severe flooding in Western Europe during July 2021, URL: <https://www.worldweatherattribution.org/heavy-rainfall-which-led-to-severe-flooding-in-western-europe-made-more-likely-by-climate-change/>
- Nasreen, S., Součková, M., Vargas Godoy, M. R., Singh, U., Markonis, Y., Kumar, R., Rakovec, O., and Hanel, M.: A 500-year runoff reconstruction for European catchments, *Earth Syst. Sci. Data Discuss.* [preprint], <https://doi.org/10.5194/essd-2021-282>, in review, 2021.
- Roggenkamp, T. and Herget, J., 2014. Reconstructing peak discharges of historic floods of the River Ahr, Germany. *Erdkunde*, pp.49-59 (doi: 10.3112/erdkunde.2014.01.05)
- Shen, C., 2018. A transdisciplinary review of deep learning research and its relevance for water resources scientists. *Water Resources Research*, 54(11), pp.8558-8593.
- Schulzweida, U., et al. 2020. CDO user's guide. Climate Data Operators, MPI for Meteorology, <https://code.mpimet.mpg.de/projects/cdo/embedded/cdo.pdf> (accessed: 9.6.2021)
-

Expected date of thesis defence

2022/23 SS – FES

The Bachelor Thesis Supervisor

Ing. Oldřich Rakovec, Ph.D.

Supervising department

Department of Water Resources and Environmental Modeling

Electronic approval: 6. 3. 2023

prof. Ing. Martin Hanel, Ph.D.

Head of department

Electronic approval: 22. 3. 2023

prof. RNDr. Vladimír Bejček, CSc.

Dean

Prague on 30. 03. 2023

STATEMENT

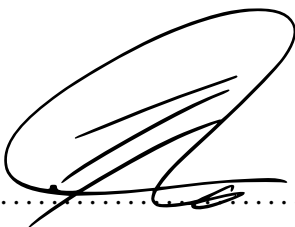
I hereby declare that I have independently elaborated the bachelor/final thesis with the topic of: **”Reconstructing of the German summer floods 2021 using the data-driven methods”** and that I have cited all of the information sources that I used in the thesis as listed at the end of the thesis in the list of used information sources.

I am aware that my bachelor/final thesis is subject to Act No. 121/2000 Coll., on copyright, on rights related to copyright, and on amendments of certain acts, as amended by later regulations, particularly the provisions of Section 35(3) of the act on the use of the thesis.

I am aware that by submitting the bachelor/final thesis I agree with its publication under Act No. 111/1998 Coll., on universities and on the change and amendments of certain acts, as amended, regardless of the result of its defense.

With my own signature, I also declare that the electronic version is identical to the printed version and that the data stated in the thesis has been processed in relation to the GDPR.

Prague March 30, 2023

A handwritten signature in black ink, consisting of a large, stylized initial 'R' followed by a horizontal line and a small flourish at the end. The signature is positioned above a dotted line.

Ronak Rahmati

ABSTRACT

Heavy rains caused floods in the Eifel/Ahr region of Germany on July 14–15, 2021, killing 184 people and severely damaging infrastructure such as houses, roads, and communications. Under current climatic conditions, a similar event is expected to occur approximately every 400 years in certain parts of Western Europe. This thesis aims to quantify the ability of two existing data-driven (Neural Network) and one hydrological (GR6J) model to reconstruct the record-breaking flood events, which was caused by daily rainfall accumulation exceeding 100 mm. We have used observed precipitation and temperature data derived from different meteorological data sets and observed discharge time series on the Ahr river basin to set up and run the Neural Network (BRNN and LSTM) and hydrological (GR6J) models for the period 1992–2021. The first half was used for calibration/model training and the latter half was used for independent evaluation. The comparison of simulated results to observed discharge data has shown that the GR6J results outperform the simulations of the BRNN and LSTM setups, particularly in the validation period across all four meteorologic forcing data sets. However, if the data-driven models (BRNN and LSTM) are trained on high daily accumulations and exceptional flood peaks, they can capture flood signals and, in some cases, the flood apex.

Key words: floods; model setup; neural network; data analysis; GR6J; brnn; July 2021; Ahr.

ABSTRAKT

Přívalové deště způsobily v německém regionu Eifel/Ahr ve dnech 14.-15. července 2021 záplavy, při nichž zahynulo 184 lidí a byla vážně poškozena infrastruktura, například domy, silnice a komunikace. Za současných klimatických podmínek se očekává, že k podobné události dojde v některých částech západní Evropy přibližně jednou za 400 let. Cílem této práce je kvantifikovat schopnost dvou existujících datově řízených (neuronová síť) a jednoho hydrologického (GR6J) modelu rekonstrukci rekordních povodní, které byly způsobeny denním úhrnem srážek přesahujícím 100 mm. K sestavení a spuštění neu-

ronové sítě (BRNN a LSTM) a hydrologického modelu (GR6J) pro období 1992–2021 jsme použili pozorované údaje o srážkách a teplotě získané z různých meteorologických datových sad a pozorované časové řady odtoku v povodí řeky Ahr. První polovina byla použita pro kalibraci/trénování modelů a pozdější polovina pro nezávislé vyhodnocení. Srovnání simulovaných výsledků s pozorovanými údaji o odtoku ukázalo, že výsledky modelu GR6J překonávají simulace sestav BRNN a LSTM, zejména v ověřovacím období ve všech čtyřech souborech meteorologických podnětů. Pokud jsou však modely založené na datech (BRNN a LSTM) vycvičeny na vysokých denních akumulacích a výjimečných povodňových špičkách, mohou zachytit povodňové signály a v některých případech i vrchol povodně.

Klíčová slova: povodně; sestavení modelu; neuronová síť; analýza dat; GR6J; brnn; červenec 2021; Ahr.

List of Figures

2.1	Topographic map of the Altenahr Ahr basement in Germany	6
2.2	Monthly climatology for precipitation based on four different meteorological data sets (ERA5-Land, EMO-1arcmin, E-OBS, and REGNIE) over 30 years (1992–2021).	9
2.3	Monthly climatology for temperature based on different meteorological data sets (ERA5-Land, EMO-1arcmin, E-OBS, and REGNIE) over 4 decades (1980–2021).	10
2.4	Annual daily precipitation trends for ERA5-Land, EMO-1arcmin, E-OBS, and REGNIE data sets over 40 years (1980–2021). The trend line is highlighted in orange in the graphs.	11
2.5	Temperature trends for ERA5-Land, EMO-1arcmin, E-OBS, and REGNIE data sets over 40 years from 1980 to 2021. The trend line is highlighted in orange in the graphs.	12
2.6	Seasonality of monthly observed discharge over 30 years (1992–2021).	14
2.7	Trend of observed discharge over 30 years (1992–2021). The trend line is highlighted in orange.	15
2.8	Schematization of the biological and artificial Neuron, taken from Singh (2018).	17
2.9	Diagram of bidirectional recurrent neural networks taken from Jokar and Semperlotti (2020).	18
2.10	Schematization of the Long short-term memory (LSTM) cell, taken from Saxena (2021).	20

3.1	Hydro-graph of training (top) and testing (bottom) period by BRNN model for ERA5-Land.	27
3.2	The seasonality of simulated discharge by BRNN model based on four data sets (ERA5-Land, EMO-1arcmin, E-OBS, and REGNIE) against observed discharge over 30 years (1992–2021), including both the training and testing periods.	28
3.3	Hydrograph at the top: as training and at the bottom: as testing period by LSTM model for EMO-1arcmin.	29
3.4	The seasonality of simulated discharge by LSTM model using four different data sets (ERA5-Land, EMO-1arcmin, E-OBS, and REGNIE) against observed discharge over 3 decades (1992–2021), including the training and testing periods.	30
3.5	Hydro-graph of calibration (top) and evaluation (bottom) period by GR6J model for REGNIE data set.	32
3.6	The seasonality of simulated discharge by GR6J model based on four meteorological data sets (ERA5-Land, EMO-1arcmin, E-OBS, and REGNIE) against observed discharge over 30 years (1992–2021) including both, the training and testing periods.	33
3.7	The cumulative precipitation based on four meteorological data sets (ERA5-Land, EMO-1arcmin, E-OBS, and REGNIE) in year 2021.	34
3.8	Hydro-graph of calibration results for BRNN (top), LSTM (middle), and GR6J (bottom) in 2021 for four meteorological data (ERA5-Land, EMO-1arcmin, E-OBS, and REGNIE).	39

List of Tables

3.1	BRNN results for training and testing periods at daily time steps using precipitation and temperature based on different meteorological data sets (ERA5-Land, EMO-1arcmin, E-OBS, and REGNIE) as input.	28
3.2	LSTM results for training and testing periods at daily time steps using precipitation and temperature from four different data sets (ERA5-Land, EMO-1arcmin, E-OBS, and REGNIE) as input.	31
3.3	GR6J model results for calibration (training) and evaluation (testing) periods using precipitation and potential evapotranspiration based on four different data sets (ERA5-Land, EMO-1arcmin, E-OBS, and REGNIE) as inputs at daily time steps.	33
3.4	BRNN model results for the flood peak of July 14 to 16, 2021 based on four meteorological data sets (ERA5-Land, EMO-1arcmin, E-OBS, and REGNIE) against observed discharge. All the values are in cubic meters per second (m ³ /s).	35
3.5	Results from the LSTM model based on four different data sets (ERA5-Land, EMO-1arcmin, E-OBS, and REGNIE) for the flood peak of July 14 to 16, 2021 against observed discharge. All measurements are in cubic meters per second(m ³ /s).	36
3.6	The results of the GR6J model based on different meteorological data (ERA5-Land, EMO-1arcmin, E-OBS, and REGNIE) for the flood peak of July 14 to 16, 2021 against observed discharge. All measurements are in cubic meters per second. (m ³ /s).	36

Contents

1 Introduction	1
2 Methodology	5
2.1 Description Of The Study Domain	5
2.2 Overview Meteorological Data Set	6
2.2.1 E-OBS	6
2.2.2 REGNIE	7
2.2.3 EMO-1arcmin	7
2.2.4 ERA5-Land	7
2.3 Long-term Statistics For Meteorological Data Set	8
2.3.1 Monthly Climatology Of Precipitation	8
2.3.2 Monthly Climatology Of Temperature	10
2.3.3 Precipitation Trends In The Annual Mean Values	11
2.3.4 Temperature Trends In The Annual Mean Values	12
2.4 Observed Hydrological Data	13
2.4.1 Stream-Flow - Q	13
2.4.2 Monthly Climatology Of Observed Stream-Flow - Q	13
2.4.3 Stream-Flow - Q Trends In The Annual Mean Values	14
2.5 Modelling	15
2.5.1 Neural Network Model	16
2.5.2 Bidirectional RNN (BRNN)	18
2.5.3 Long Short-Term Memory (LSTM)	19
2.5.4 GR6J Hydrological Model	21

3 Results And Discussions 25

3.1 Development And Testing Of NNM Model With BRNN Architecture . . 25

3.2 Development And Testing Of NNM Model With LSTM Architecture . . . 26

3.3 Development And Testing GR6J Hydrological Model 31

3.4 Evaluation Of The Modeling Results For The Flood Peak Of July 2021
(As Testing Period) 34

3.5 Evaluation Of The Modeling Results For The Flood Peak Of July 2021
(As Training Period) 37

4 Conclusion And Future Work 41

Chapter 1

Introduction

Due to global warming, the climate is changing all over the world, and it is also changing in Europe. It is projected that climate change will cause unexpected, unusual, severe, or unseasonal weather events, such as heavy rainfall, floods, heat waves, tornadoes, droughts, etc. According to the sixth Intergovernmental Panel on Climate Change (IPCC) assessment report (Legg, 2021) heavy precipitation and consequently riverine flooding have been raised in Western and Central Europe in recent decades as a result of global warming. With reference to Kreienkamp et al. (2021) if global warming due to rising greenhouse gas emissions reaches 2 degrees Celsius by mid-century, as already expected, Europe may encounter harsher weather phenomena, such as a rise in heavy rainfall and river flooding, even in the warm months when the amount of wet days is expected to decrease. Although the frequency of wet days may lessen, the severity of extreme rain showers might escalate, leading to a greater possibility of intense weather events. (Menne et al., 2013). This was exactly the same scenario as what occurred in Germany and neighboring countries during the period of July 14–15, 2021.

After above-average rainfall in June 2021 and repeated rainfall in early July, warm and very moist air masses moved from the Mediterranean region into southwestern Germany, resulting in persistent rain on July 13 and 14. As stated by Mohr et al. (2022) the extremely heavy and continuous rain combined with the already high soil moisture levels resulted in a catastrophic destructive flash flood on July 14-15 in the northern part of the low mountain range Eifel and affected the villages along the rivers Ahr and Erft. According to a study by World Weather Attribution (Kreienkamp et al., 2021), a similar event is expected to occur

approximately every 400 years in certain parts of Western Europe under current climatic conditions. The disaster led to 184 fatalities and significant damage to infrastructure such as houses, roads, communication, etc in Germany. As reported by [Munich Re \(2022\)](#) the total damage in Germany was estimated to be around €33 billion, making the event the most expensive disaster in German history. The majority of the deaths occurred in the Ahr valley, which runs 25 miles (40 kilometers) south of Bonn to where the river joins the Rhine. According to the Ahrweiler administrative district report ([Truedinger et al., 2023](#)), approximately 56 000 people live actively on the Ahr River, and nearly 42 000 of these people were negatively affected by the July 2021 flood.

In the opinion of [Ye et al. \(2020\)](#) efficient and effective emergency management is critical to mitigating the negative impacts of disasters, especially in the case of sudden natural disasters. A prerequisite for disaster preparedness is to identify the most vulnerable infrastructure and areas, prioritize emergency response, and organize evacuations if needed, by measuring the scale and extent of the event in the most accurate and timely manner possible. Anticipating such unexpected extremes challenges the prediction chain and opens new avenues for rethinking long-standing questions ([Wang et al., 2011](#)). How reliable and accurate are current models in predicting unexpected floods?

The catastrophic effects of the July flood in 2021 provide the impetus for an event attribution analysis to investigate the efficacy of the existing data-driven (Neural network) model and hydrological (GR6J) model in predicting unexpected flood events. Since a recent study by [Saadi et al. \(2023\)](#) demonstrated that the accuracy of the recorded precipitation can affect the accuracy of the model, this study is conducted under the assumption that the recorded data provided by different data sets have the same accuracy. The main objectives are to investigate how well data-driven approaches can reconstruct the scale of flooding that occurred during the destructive floods in the Ahr River basin (Germany) in the summer of 2021. Additionally, the study will examine the impact of meteorological uncertainty on the reconstruction process. The results will be additionally compared against a simple conceptual model of a predefined model structure using six calibration parameters.

This thesis is followed by a description of the study domain (Section [2.1](#)), an overview

of the meteorological data sets (Section 2.2), an evaluation of long-term statistics (Section 2.3), analyzing the observed stream-flow (Section 2.4), a brief definition of the applied models (Section 2.5), development and testing of BRNN model (Section 3.1). Results of the development and testing of LSTM model (Section 3.2), development and testing of GR6J hydrological model (Section 3.3), evaluation of the models as testing period (Section 3.4), evaluation of the models as training period (Section 3.5), and finally the conclusion are included in (Section 4).

Chapter 2

Methodology

This section is organized into several subsections. First, basin short description (Section 2.1); second, different meteorological data sources are described (Section 2.2); third, long-term statistics are quantified, such as monthly climatology and annual trends (Section 2.3). Next, observed stream-flow climatology and trends are analyzed (Section 2.4). Finally, a description of the models used to simulate hydrological response is provided (Section 2.5).

2.1 Description Of The Study Domain

The Ahr River is an 85-kilometer-long left tributary of the Rhine in Western Germany (figure 2.1). In accordance with Campana et al. (2012) the Ahr River has a catchment area of approximately 900 km² and sources from the Eifel mountains near Blankenheim, at an elevation of around 470 meters above sea level (Roggenkamp and Herget, 2014). As determined by U.S. Geological Survey (2018), the Ahr basin has a maximum elevation of 716 meters and a minimum elevation of 51 meters above sea level. While the average bottom gradient in the middle and lower reaches is not particularly steep, parts of the catchment are above 600 m asl, making the entire catchment area vulnerable to surface runoff intensification (Szymczak et al., 2022). The geological foundation of the basin is dominated by shale rocks which prevent water from penetrating deeper layers (Campana et al., 2014). The lower valley of the Ahr basin has a U-shaped section carved by glaciers and strongly influences Ahr's stream-flow. Because of these morphological characteristics, villages adjacent to the Ahr are at risk of flood damage. As stated by Truedinger et al.

(2023) approximately 56 000 people live actively on the Ahr River, and according to the Ahrweiler administrative district report, nearly 42 000 of these people were negatively affected by the flood on July 2021.

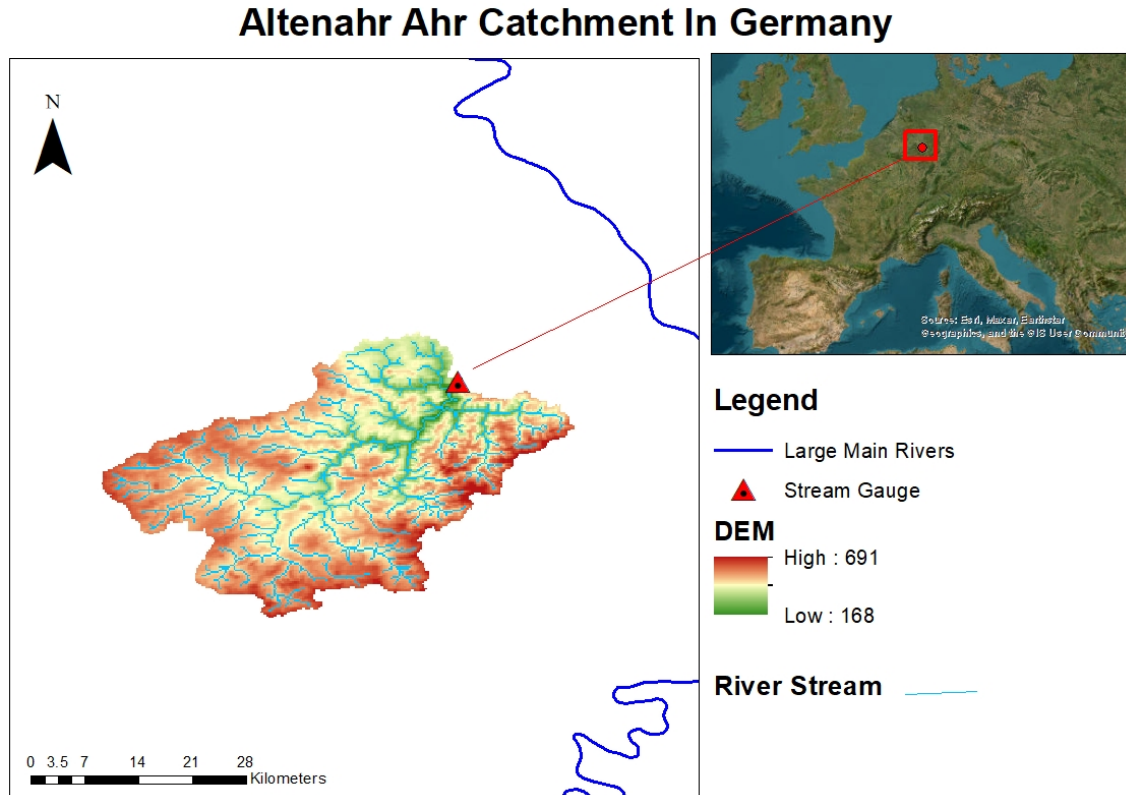


Figure 2.1: Topographic map of the Altenahr Ahr basement in Germany

2.2 Overview Meteorological Data Set

2.2.1 E-OBS

E-OBS is a land-only observational data set with a daily temporal resolution that is available at two spatial resolutions of $0.25^\circ \times 0.25^\circ$ and $0.1^\circ \times 0.1^\circ$ at regular grid over Europe covering the area 25°N – 71.5°N , 25°W – 45°E (Cornes et al., 2018). E-OBS has been derived from meteorological stations across Europe that are sourced from the European National Meteorological and hydro-logical Services (NMHSs) or other data-holding associations (Klein Tank et al., 2002; Klok and Klein Tank, 2009). The data set covers the period from the 1st of January 1950 to the near real-time and is updated constantly and provides information on various meteorological factors, such as the daily minimum temperature

(TN), daily maximum temperature (TX), daily average temperature (TG), daily total precipitation (RR), daily average wind speed (FG), daily mean sea level pressure (PP), daily average relative humidity (HU), and global radiation (QQ) (Cornes et al., 2018). The E-OBS data set is publicly available from E-OBS database (2023).

2.2.2 REGNIE

REGNIE is a daily rainfall data set with a horizontal resolution of $1 \text{ km} \times 1 \text{ km}$ over Germany (Kreienkamp et al., 2021). As stated by Kaspar et al. (2015) this data set is derived from station data provided by the German Meteorological Service since the 1st of January 1931. REGNIE data set is available for public use in a format of arc-Files of one year from REGNIE database (2023).

2.2.3 EMO-1arcmin

EMO-1arcmin is a multi-variable meteorological data set from Europe with a 1 km spatial resolution and daily period (Thiemig et al., 2022). This data set is made on historical and real-time observations and covers the period from 1990 to 2019 (Kakoulaki et al.), but regular updates until 2022 can be found on the data repository. The EMO-1arcmin is a product of Copernicus Emergency Management Service and provides daily resolution data for total precipitation, solar radiation, minimum temperatures, maximum temperatures, wind speed, and water vapor pressure (Thiemig et al., 2022). Furthermore, the data for precipitation and the mean temperature is available by this data set every 6 hours. The EMO-1arcmin data set is publicly available from EMO-1arcmin database (2023) as a product of Copernicus.

2.2.4 ERA5-Land

The ERA5-Land is a reanalysis data set providing a constant view of the transition of land variables (Muñoz-Sabater, 2021). This data set supplies hourly high-resolution information on surface variables from 1950 to 2-3 months before the present. ERA5-Land

has been created by replacing the land component of the ERA5 climate reanalysis with a better spatial resolution: approximately 9 km (0.08) grid spacing (Muñoz Sabater, 2019).

According to Muñoz-Sabater (2021) and Jeppesen (2021), reanalysis uses the laws of physics and fills the gaps in the observational record by merging the model data with observations from all around the world and producing a universally complete and consistent data set. Created data by Reanalysis go several decades back in time and provide a precise description of the weather and climate of the past.

ERA5-Land supplies data for a total of 50 variables such as 2m dew-point temperature, 2m temperature, evaporation from bare soil, potential evaporation, runoff, total evaporation, total precipitation, etc. Accordant with Jeppesen (2021) at reduced spatial and temporal resolutions, ERA5-Land contains information for all variables about uncertainties (data from locations or periods where observations are scanner are possible to be less confident).ERA5-Land is very convenient for all types of land surface applications like overflow or drought forecasting due to its temporal and spatial resolutions (Muñoz-Sabater, 2021). The latest ERA5-Land data set is available free of charge from ERA5-LAND database (2023) either in GRIB1, GRIB2, or netCDF format.

2.3 Long-term Statistics For Meteorological Data Set

2.3.1 Monthly Climatology Of Precipitation

Figure 2.2 shows the monthly mean of precipitation for observational data provided by four different data sets (ERA-5Land, E-OBS, REGNIE, and EMO-1arcmin) over 30 years (1992–2021). The precipitation data in the y-axis is in millimeter (mm) scale and for all data sets except ERA5-Land is recorded in a similar range. For E-OBS, REGNIE, and EMO-1arcmin, the lowest recorded rainfall is between 49 mm and 52 mm, and the highest recorded amount is between 74 mm and 76 mm, whereas for ERA5-Land, the minimum recorded precipitation is around 60mm, and the maximum recorded value exceeds 90mm, indicating that ERA5-Land consistently overestimates the values. The highest amounts of precipitation are recorded during the summer and winter seasons, and the least values are captured during the spring and autumn.

The CDO codes below include the required Climate Data Operators by Schulzweida

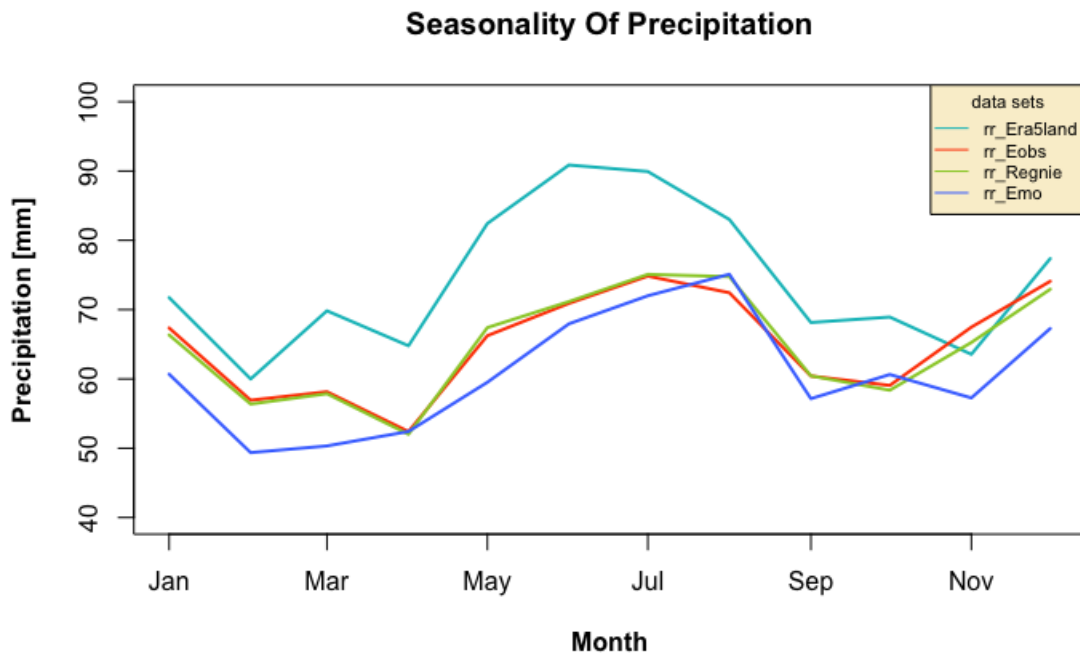


Figure 2.2: Monthly climatology for precipitation based on four different meteorological data sets (ERA5-Land, EMO-1arcmin, E-OBS, and REGNIE) over 30 years (1992–2021).

et al. (2006) to process the precipitation data for monthly climatology in figure 2.2. In this operation, the data over the Ahr basin was averaged over all grid cells and the resulting data were used to compute the mean precipitation for each month over a 40-year period (1980–2021).

```
# Step1: Calculate the average over all grid cells
cdo fldmean input_Pr.nc fldmean_Pr_output.nc

# Step2: Calculating the monthly sum of the precipitation
cdo monsum fldmean_Pr_output.nc monsum_Pr_output.nc

# Step3: Calculating the yearly mean of each month
cdo ymonmean monsum_Pr_output.nc ymonmean_Pr_output.nc
```

2.3.2 Monthly Climatology Of Temperature

Figure 2.3 shows the monthly mean of temperature for observational data from three different data sets (ERA-5Land, E-OBS, and EMO-1arcmin) over 40 years period from 1980 to 2021. The temperature data in the y-axis is given in degree Celsius units. The recorded data of E-OBS and EMO-1arcmin display a similar range of temperature while Era5-Land stays a little further away due to the clear existing seasonality with reference to figure 2.2. Because the ERA5-Land was more wet, the temperature is also lower. The maximum temperature recorded by the two data sets E-OBS and EMO-1arcmin is around 16 C° and 17 C°, respectively, while the highest temperature recorded by ERA5-Land does not even reach 15 C°.

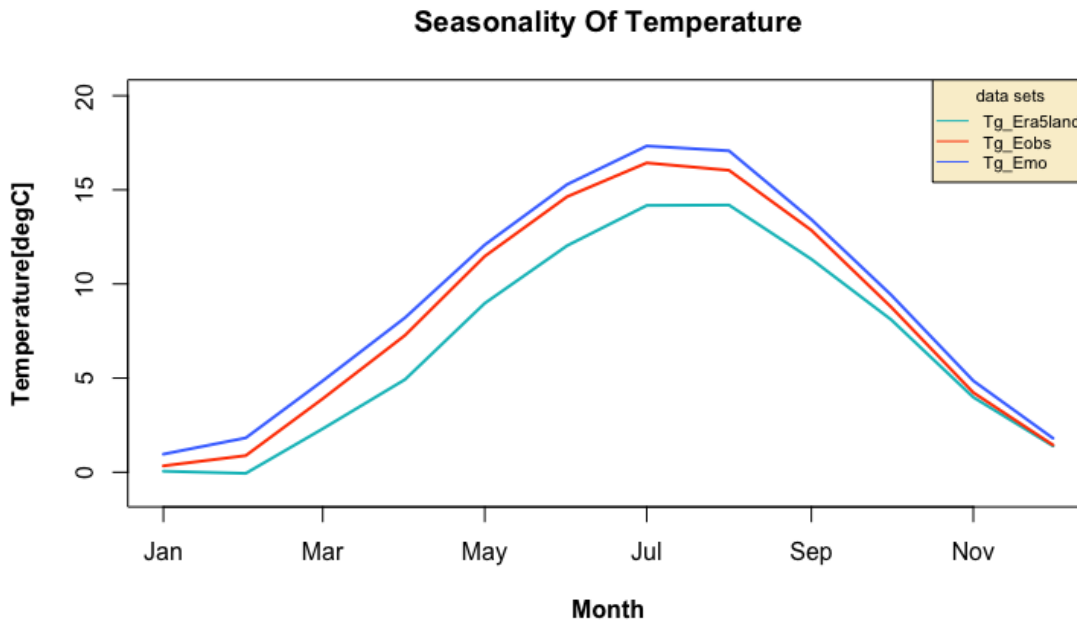


Figure 2.3: Monthly climatology for temperature based on different meteorological data sets (ERA5-Land, EMO-1arcmin, E-OBS, and REGNIE) over 4 decades (1980–2021).

The following CDO codes provide the needed Climate Data Operators to process the temperature data for monthly climatology in figure 2.3. During the procedure, the temperature data over the Ahr basin was calculated for the mean over all grid cells and the result was used to measure the mean temperature for each month over 40 years (1980–2021).

```
# Step1: Calculate the average over all grid cells
```



```
cdo fldmean input_tem.nc fldmean_tem_output.nc
```

```
# Step2: Calculating the yearly mean of each month
```

```
cdo ymonmean fldmean_tem_output.nc ymonmean_tem_output.nc
```

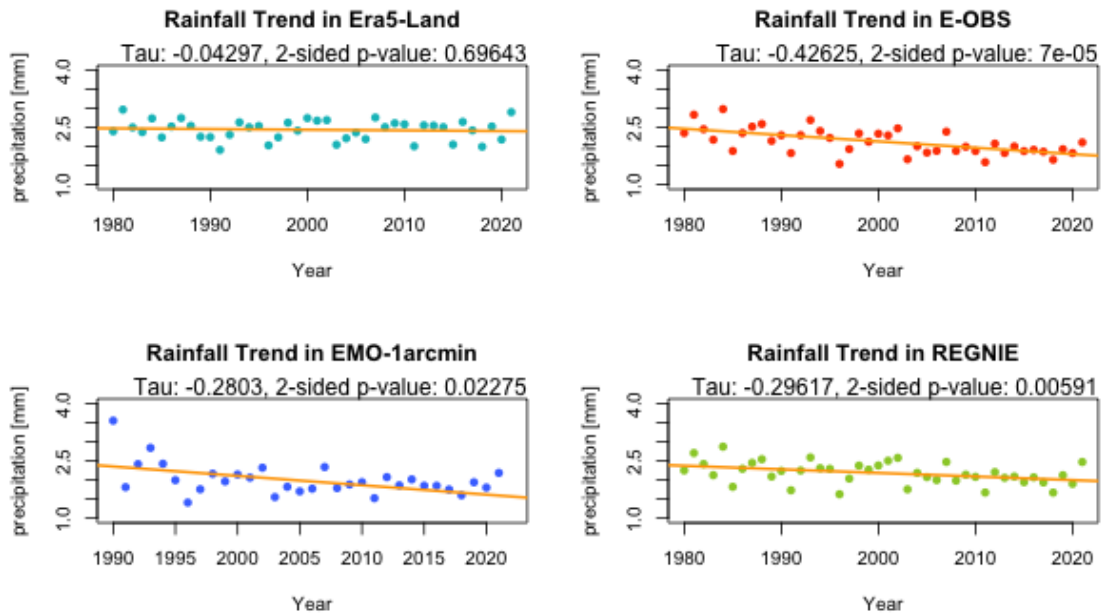


Figure 2.4: Annual daily precipitation trends for ERA5-Land, EMO-1arcmin, E-OBS, and REGNIE data sets over 40 years (1980–2021). The trend line is highlighted in orange in the graphs.

2.3.3 Precipitation Trends In The Annual Mean Values

Figure 2.4 shows the trends in the annual mean values for precipitation data provided by four different data sets (Era5-Land, E-OBS, EMO-1arcmin, and REGNIE) based on Mann-Kendall Trend Test (McLeod, 2005). The Mann-Kendall (MK) test is used in conjunction with linear regression analysis to determine whether the slope of the estimated linear regression line is greater/less than zero and whether the variable of interest has a monotonic upward or downward trend over time. This method primarily provides two different kinds of information:

1. The Kendall Tau, also known as the Kendall rank correlation coefficient, assesses the monotony of the slope.

2. The Significance, which represents the point at which the hypothesis of no trend is accepted. When the p-value is less than 0.05, the trend is statistically considerable.

Concerning the Significance of the MK test, the null hypothesis of no monotonic trend is rejected for all data sets (E-OBS, EMO-1arcmin and REGNIE) except ERA-Land, which has a higher p-value than 0.05 . Negative Kendal Tau values indicate a downward trend in precipitation from 1990 to 2021 for E-OBS, EMO-1arcmin and REGNIE data sets.

49

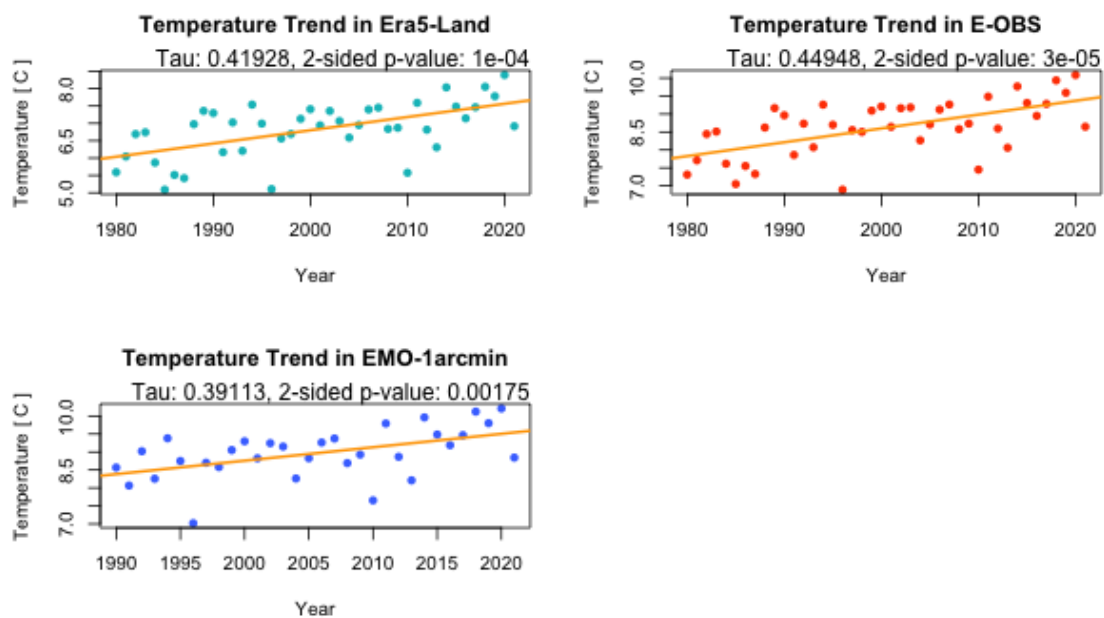


Figure 2.5: Temperature trends for ERA5-Land, EMO-1arcmin, E-OBS, and REGNIE data sets over 40 years from 1980 to 2021. The trend line is highlighted in orange in the graphs.

2.3.4 Temperature Trends In The Annual Mean Values

Figure 2.5 displays the Mann-Kendall Trend Test for annual mean values of temperature data from three different data sets (Era5-Land, E-OBS, and EMO-1arcmin). The Mann-Kendall (MK) test, in addition to linear regression analysis, is applied to decide whether the slope of the estimated linear regression line shows an upward or downward trend over the given period. Correspondingly for all three data sets the MK test's Significance rejects

the null hypothesis of no monotonic trend, and since $p - values < 0.05$, the Kendal Tau suggests an upward trend in temperature for the relevant timeline.

2.4 Observed Hydrological Data

2.4.1 Stream-Flow - Q

[Rhineland-Palatinate \(2021\)](#) provides discharge data (Q [m^3/s]) for the Ahr basin, a major tributary of the Rhine river with a catchment area of $747,087 \text{ km}^2$, in 15-minute temporal resolution in the form of a text file (CSV file) or an Excel spreadsheet (XLS file). This data can be retrieved for a maximum of 30 days. In this paper, the data is aggregated into daily values for subsequent analysis.

The following R-code is used to convert the 15-minute recorded data of Ahr basin discharge to daily outflow. The result of aggregation shows that the minimum and maximum outflow in the Ahr basin over the last 30 years was $0.415 \text{ (m}^3/\text{s)}$ and $465.3125 \text{ (m}^3/\text{s)}$ during 2017-07-09 and 2021-07-15, respectively.

```
# Required Libraries
library(dplyr)
library(lubridate)

# Aggrigating the daily mean of discharge
daily_mean <- discharge_df %>%
  group_by(Date) %>%
  summarize(dilyMean = mean(Q))
```

2.4.2 Monthly Climatology Of Observed Stream-Flow - Q

Figure [2.6](#) represents the average value of the observed discharge in each month over a 30-year time frame. The plotted data indicates that discharge is higher during the winter season and decreases as it gets closer to summer.

To demonstrate seasonality, the data was processed in R as follows to convert daily outflow to monthly averaged discharge.

```
# Required Libraries
library(dplyr)
library(lubridate)

# Convert the daily mean to ymonmean
monthly_mean <- discharge_df %>%
  group_by(month) %>%
```

```
summarize(ymonmean = mean(dailyMean))
```

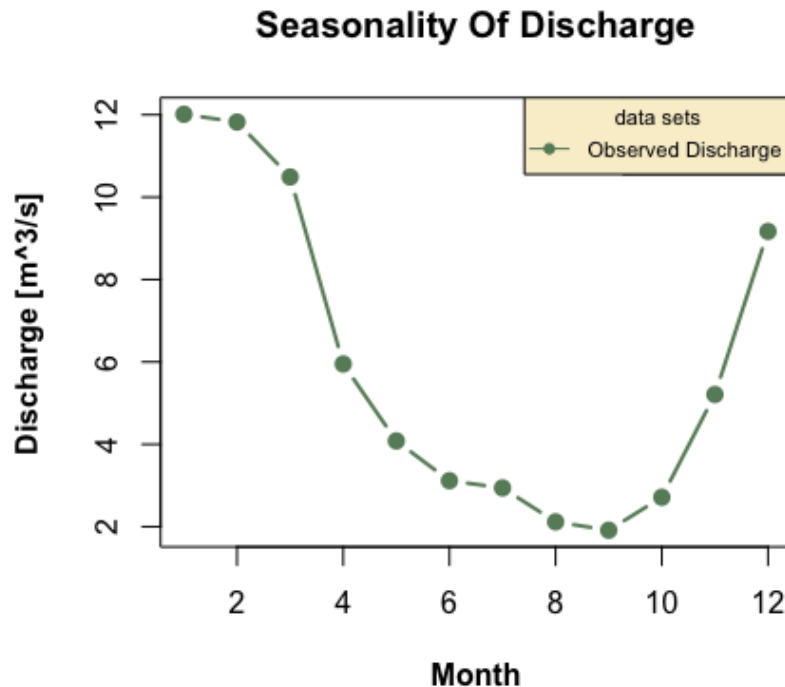


Figure 2.6: Seasonality of monthly observed discharge over 30 years (1992–2021).

2.4.3 Stream-Flow - Q Trends In The Annual Mean Values

Figure 2.7 presents the Mann-Kendall Trend Test in annual daily mean values for observed discharge data. Even though the linear regression shows a monotonic bearish trend over time, the significance of the Mann-Kendall Trend Test cannot reject the null hypothesis of no monotonic trend for outflow.

The R-code below reveals how to process daily discharge to obtain the yearly averaged outflow required for the Kendal trend test.

```
# Required Libraries
library(dplyr)
library(lubridate)

# Convert the daily mean[m^3/s] to yearly mean[mm/day]
yearly_mean <- discharge_df %>%
  group_by(year) %>%
  summarize(yearlyMean =
    (mean(dailyMean) * (1000*24*3600) / 747000000))
```

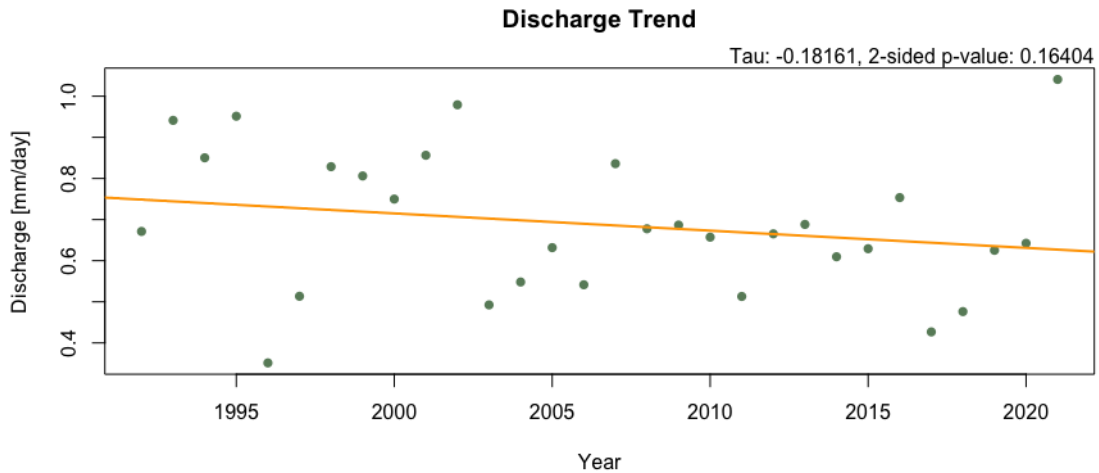


Figure 2.7: Trend of observed discharge over 30 years (1992–2021). The trend line is highlighted in orange.

2.5 Modelling

This section investigates several tools for simulating hydrological response to meteorological inputs, with a particular focus on representing the dramatic floods of July 14 and 15, 2021 in the Ahr basin. This thesis uses data-driven models such as Neural Network Modeling (NNM) as well as a hydrological model like the GR6J rainfall-runoff modeling, and tests and evaluates their accuracy. The selection of these models was inspired by the recent work of [Nasreen et al. \(2022\)](#), who used the models to predict annual river flows for 14 European catchments, while models here are used to simulate daily flows of the Ahr River.

The temperature and precipitation data from E-OBS, REGNIE, EMO-1arcmin, and ERA5-Land were collected over 30 years on the Ahr basin and are used to run the corresponding models. Each data set is divided into halves to define the training and testing periods. For each model, the first half (1992–2007) is used for training and the second half (2008–2021) is used for testing. The selected objective function for constraining the model parameters of the BRNN and GR6J models was based on the root mean square (RMSE), while for LSTM this was based on the mean squared error (MSE). We assume this does not have a large difference for the simulated results, moreover, since several other objective functions are used for evaluating the model performance. In the first part of

the analysis, the overall hydrological response is summarized (and differences stemming from different meteorological products are documented), in the second half of the analysis, we assess, how the models can capture the peak of July 2021. The R-code below demonstrates the steps of creating the required training and testing periods for the models.

This work is based on the code presented earlier by [Nasreen et al. \(2022\)](#).

```
# steps to split the data into training and testing periods:
#1) pr and tem data for the training period
meteo_training<-data[1: floor(0.5*nrow(data),
c('pr','tem') ]
#2) pr and tem data for the testing period
meteo_testing<- data[ (floor(0.5*nrow(data)+1):nrow(data),
c('pr','tem') ]
#3) discharge data for the training period
Qobs_training <- data[1: floor(0.5*nrow(data),
.(Q_m3) ]
#4) discharge data for the testing period
Qobs_testing <- data[ (floor(0.5*nrow(data)+1):nrow(data),
.(Q_m3) ]
```

2.5.1 Neural Network Model

Neural networks, also known as artificial neural networks (ANNs), are a branch of machine learning that form the foundation of deep learning algorithms. Their name and framework are derived from the human brain, and they work in the same way that biological neurons do ([Abraham, 2005](#)) as it is shown in the figure [2.8](#). Neurons are the fundamental units of artificial neural networks (ANNs), which are typically structured into layers. As stated by [Jain et al. \(1996\)](#) the arrangement of a neural network comprises three layers, namely, an initial layer composed of units representing the input fields, one or more hidden layers, and a concluding layer featuring one or multiple units that represent the target field(s). The units are connected using a variety of connection strengths (or weights). The first layer receives input data, and if any individual neuron's output exceeds a predefined threshold value, that neuron is amplified and sends data to the network's next layer ([Zou et al., 2009](#)). If this is not the case, no data is transferred to the next network layer. Finally, the output layer generates a result. Accordant with [Benton et al. \(2020\)](#) training data is used by neural networks to learn and enhance their precision over time by evaluating individual records, creating a prediction for each record, and adjusting the weights when it makes an invalid prediction. This process is repeated many times, and the

network's predictions improve until one or more of the stopping criteria are met. Today, different kinds of artificial neural networks are used in machine learning. However, Recurrent Neural Networks (RNN) are among the most popular. An RNN is a kind of artificial neural network that uses sequential or time series data and works on the principle of saving a layer's output and feeding it into the input to help predict the layer's outcome (Maladkar, 2018). This means that each neuron will memorize some data from the prior time step as it moves from one-time step to the next. This causes each neuron to function as a memory cell when performing computations. For different purposes, RNN provides users with a variety of architectures including Bidirectional RNNs (BRNN), Long short-term memory (LSTM), and Gated recurrent units (GRUs). In this paper, BRNN and LSTM architectures of RNN are used to represent the hydrological cycle over the last 30 years in the Ahr basin.

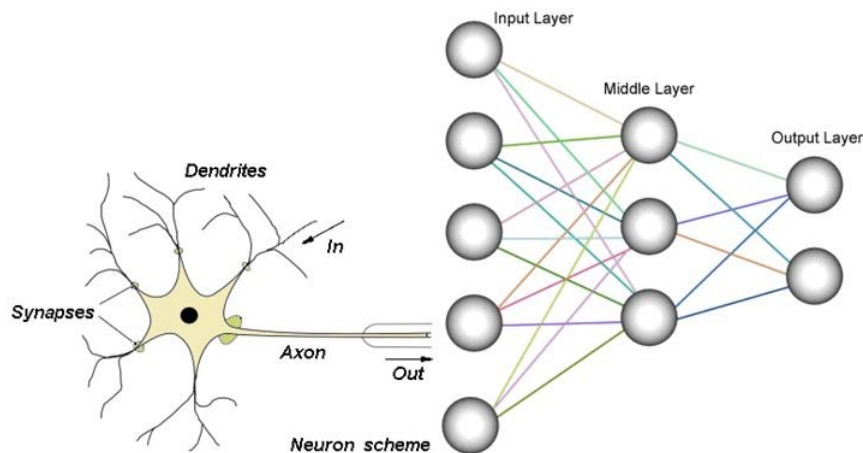


Figure 2.8: Schematization of the biological and artificial Neuron, taken from Singh (2018).

Figure 2.8 displays the similarity between biological and artificial neural networks. The left side of the image above represents a biological neuron, and the right side represents the links of multiple nodes (neurons) in ANN. Because ANN is based on the structure of a biological neural network (BNN), it resembles BNN in appearance. They are both made up of neurons (BNN consists of neurons as cells and ANN consists of neurons as nodes). Multiple neurons use electricity to transmit and receive data points from their predecessors and transfer them to their descendants.

2.5.2 Bidirectional RNN (BRNN)

One of the most common RNN architectures is BRNN. BRNN is used when the user wants to explore future events without limiting the model's learning to the past and present, according to [Kastrati and Biba \(2021\)](#). As it is shown in [figure 2.9](#) a BRNN is made up of two RNNs, one of which moves forward from the beginning of the data set and the other backward from the end.

[Figure 2.9](#) shows the general structure of a BRNN model. A typical BRNN is made up of three layers: the input layer, the hidden layers, and the output layer. The diagram shows that the network's hidden layer stores two pieces of information. The two sets of RNN cells in this layer (labeled RNN F and RNN B) process the input data sequence (In_i) in opposite directions, RNNF forward (left to right) and RNNB backward (right to left). In the final output (out_n), the information from both parts is combined.

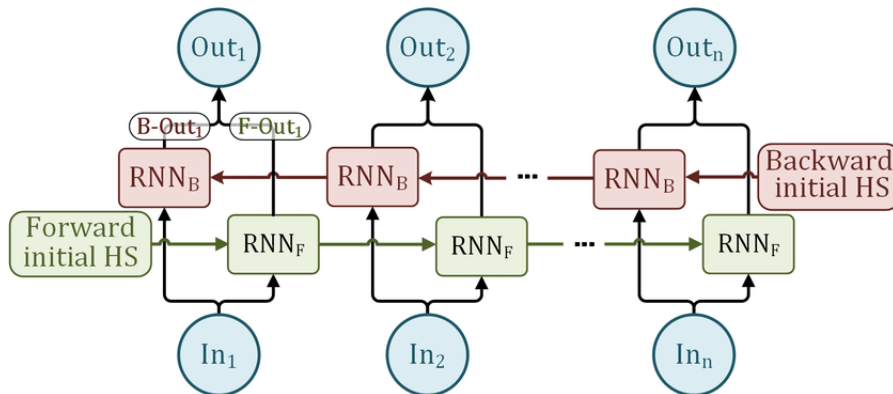


Figure 2.9: Diagram of bidirectional recurrent neural networks taken from [Jokar and Semperlotti \(2020\)](#).

In agreement with [Kuhn \(2022\)](#); [Kuhn et al. \(2020\)](#) the caret package (short for Classification And Regression Training) in R includes many functions that aim to make the model-building and analysis process as simple as possible. one of the most useful functions that are considered a key tool in this package is the train function. The train function has the ability to set up a grid of tuning parameters for so many classification and regression routines, fit each model, and evaluate a resampling-based performance measure.

The R-code below includes the train function and some of its arguments. One of the most

important arguments for this function is the method that specifies which classification or regression model to use. BRNN is one of the methods that could be used. This work is based on the code presented earlier by [Nasreen et al. \(2022\)](#).

```
# required library
library(caret)

# train function with brnn method
train(x, y,
      method = "brnn",
      ...,
      weights = NULL,
      metric = ifelse(is.factor(y), "Accuracy", "RMSE"),
      maximize = ifelse(metric == "RMSE", FALSE, TRUE),
      trControl = trainControl(),
      tuneGrid = NULL,
      tuneLength = 3)
```

Defined Arguments by [Kuhn \(2022\)](#):

`x`: a data frame containing training data where samples are in rows and features are in columns.

`y`: a numeric or factor vector containing the outcome for each sample.

`weights`: a numeric vector of case weights. This argument will only affect models that allow case weights.

`maximize`: a logical: should the metric be maximized or minimized?

`method`: a string specifying which classification or regression model to use. Possible values are: `ada`, `bag`, `bagEarth`, `bagFDA`, `blackboost`, `cforest`, `ctree`, `ctree2`.

`tuneLength`: an integer denoting the number of levels for each tuning parameter that should be generated by `createGrid`.

2.5.3 Long Short-Term Memory (LSTM)

Long short-term memory (LSTM) is an artificial recurrent neural network (RNN) architecture that allows information to be stored for a long period of time. LSTM performs similarly to an RNN cell at a high level. The internal operation of the LSTM network is shown in figure [2.10](#).

Figure [2.10](#) displays the LSTM cell's different parts (the "Cell State" the "Hidden State" and the "Gate") each of which serves a single purpose. In agreement with [Ryan \(2021\)](#) Cell State (long-term memory) provides the model with a larger memory of past events

and enables the model to store and load information from events that are not necessarily immediately preceding while the Hidden State (short-term memory) provides the model with working memory capabilities that carry information from immediately preceding events and overwrites at each step. According to [Siami-Namini et al. \(2019\)](#) the Gate is composed of three parts: The first part is known as the Forget gate, the second as the Input gate, and the third as the Output gate. As stated by [Bruneo and De Vita \(2019\)](#) each Gate serves a unique function.: the Forget gate determines if the information from the prior timestamp should be remembered or is unimportant and should be ignored. The cell attempts to learn new information from the input to this cell in the Input gate and finally, in the Output gate, the cell updates the data from the present timestamp to a subsequent timestamp. According to [Allaire and Chollet \(2023\)](#), the Keras package in R is an

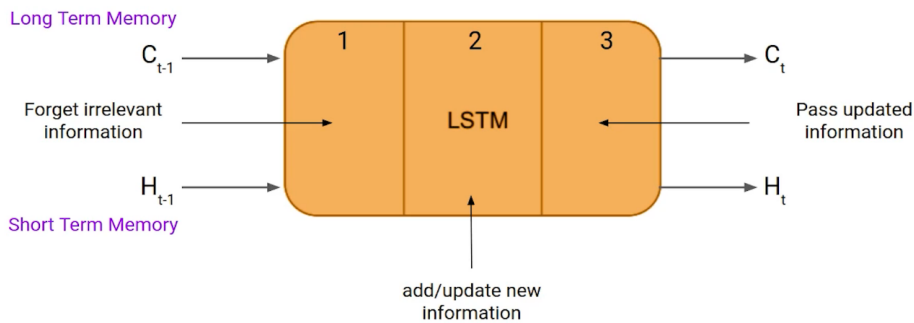


Figure 2.10: Schematization of the Long short-term memory (LSTM) cell, taken from [Saxena \(2021\)](#).

open-source Python software library that runs on top of the TensorFlow machine learning platform. Keras is a powerful interface for solving machine learning problems, with an emphasis on modern deep learning. One of Keras's most basic models is keras model sequential, which is constituted of a linear layers stack and whose learning process can be customized using the `compile ()` function of this library.

The Keras model sequential and its arguments are included in the R-code below. This work is based on the code provided by [Nasreen et al. \(2022\)](#).

```
# required library
library(keras)
library(tensorflow)
```

```

# creation of the model
model <- keras_model_sequential()
model %>%
  layer_dense(units = 32, input_shape = c(784)) %>%
  layer_activation('relu') %>%
  layer_dense(units = 10) %>%
  layer_activation('softmax')

# the configuration of the model
model %>% compile(
  optimizer = optimizer_adam(learning_rate = 0.001),
  loss = "mae",
  metrics = 'mean_squared_error'
)

```

Defined Arguments by [Allaire and Chollet \(2023\)](#):

layers: List of layers to add to the model.

name: Name of the model.

2.5.4 GR6J Hydrological Model

According to [Coron et al. \(2017\)](#) the GR6J Hydrological Model is an open-source, object-oriented model designed to simulate and analyze the hydrological behavior of river basins. This model has been developed by researchers from the French National Research Institute for Agriculture, Food and Environment, and it is based on the GR (Gridded Runoff) models that were developed in the 1980s. The development of the GR6J model was motivated by the need for an accurate and reliable hydrological model that can simulate and forecast the response of a catchment area such as runoff, soil moisture, and evapotranspiration, to different hydro-meteorological conditions ([Delaigue et al., 2018](#)). This ability of the model is achieved through the incorporation of advanced algorithms and mathematical models that take into account various factors, including precipitation, temperature, vegetation cover, soil properties, and topography. In agreement with [Delaigue et al. \(2019\)](#) the GR6J model includes several sub-models that simulate different aspects of the hydrological processes, including a rainfall-runoff model, a snowmelt model, and an evapotranspiration model. These sub-models are based on well-established and validated concepts and equations that are supported by extensive research in the field. The GR6J hydrological model uses data on a daily, monthly, and yearly time scale depending on the specific

application and data availability (Coron et al., 2018). The daily time scale is appropriate for simulating hydrological processes that exhibit short-term variability, such as rainfall-runoff processes, and for capturing the effects of climate change on water resources at a fine temporal resolution. On a daily time scale, the model considers daily variations in meteorological variables such as precipitation, temperature, and solar radiation, as well as daily changes in soil moisture and stream-flow. In keeping with Coron et al. (2022) R provides the AirGR library that implements the GR hydrological model. The package provides functions for parameter estimation, simulation, and evaluation of the model, as well as tools for sensitivity analysis and uncertainty quantification.

In the R-code example below different steps of the model setup are shown. This work is based on the code presented by Nasreen et al. (2022), previously.

```
# required library
library(airGR)

# InputsModel object
InputsModel <- CreateInputsModel
(FUN_MOD = RunModel_GR4J, DatesR = BasinObs$DatesR,
 Precip = BasinObs$P, PotEvap = BasinObs$E)
#RunOptions object
Ind_Run <- seq
(which(format(BasinObs$DatesR,
format = "%Y-%m-%d") == "1992-01-01"),
which(format(BasinObs$DatesR,
format = "%Y-%m-%d") == "2007-12-31"))
RunOptions <- CreateRunOptions
(FUN_MOD = RunModel_GR4J,
InputsModel = InputsModel, IndPeriod_Run = Ind_Run,
IniStates = NULL,
IniResLevels = NULL, IndPeriod_WarmUp = NULL)
#InputsCrit object
InputsCrit <- CreateInputsCrit
(FUN_CRIT = ErrorCrit_RMSE , InputsModel = InputsModel,
transfo=1, RunOptions = RunOptions, VarObs = "Q",
Obs = BasinObs$Q_mm[Ind_Run])
#CalibOptions object
CalibOptions <- CreateCalibOptions
(FUN_MOD = RunModel_GR4J, FUN_CALIB = Calibration_Michel)
OutputsCalib <- Calibration_Michel
(InputsModel = InputsModel, RunOptions = RunOptions,
InputsCrit = InputsCrit, CalibOptions = CalibOptions,
FUN_MOD = RunModel_GR4J)
#Simulation run
OutputsModel <- RunModel_GR4J(InputsModel = InputsModel,
RunOptions = RunOptions, Param = Param)
```

Defined Arguments By [Coron et al. \(2022\)](#):

`CreateInputsModel ()` : Prepares the inputs for the different hydrological models.

`CreateRunOptions ()` : Function allows to prepare the options required to the `RunModel*()` functions, which are the actual models functions.

`CreateInputsCrit ()` : Function allows preparing the input in order to calculate a criterion.

`CreateCalibOptions ()` : Before using the automatic calibration tool, the user needs to prepare the calibration options.

`Calibration_Michel ()` : This function allows running a calibration with the package models.

`RunModel* ()` : To run a model, the user has to use the `RunModel*()`. All the data needed have already been prepared in the previous steps.

Chapter 3

Results And Discussions

This section is organized into several sections. First, the development and testing of the BRNN model (Section 3.1); second, the development and testing of the LSTM model (Section 3.2); third, the development and testing of the GR6J hydrological model (Section 3.3); followed by evaluation of the modeling results for the flood peak (as testing period) (Section 3.4) and evaluation of the modeling results for the flood peak (as training period) in (Section 3.5).

3.1 Development And Testing Of NNM Model With BRNN Architecture

The response of the NNM with BRNN architecture for various meteorological input daily data (precipitation and temperature based on E-OBS, REGNIE, EMO-1arcmin, and ERA5-Land) on the Ahr basin over 30 years (1992–2021) is examined in this section. Each simulation was split into halves to establish the training and testing periods in order to run the model. The first half contains data from 1992 to 2007, forming the training period, and the second half includes data from 2008 to 2021, creating the testing period. In order to execute the model, the RMSE was used as the objective function.

Figure 3.1 shows the performance of the BRNN model for the training and testing periods of the ERA5-Land data set as an example. The RMSE was applied as an objective function to run the model. Kling-Gupta efficiency (KGE) and root-mean-square error (RMSE) values extracted from model performance indicate the model's prediction accuracy.

cy level. The errors or differences between observed and simulated data are lower during the training period, implying that the model is more precise in the training data set than in the testing data. This is common, since training data is based on previously learned data, whereas test data may contain unknown or uncommon data, resulting in more errors or misclassifications when performing predictions. The long-term average performance of the model to represent the stream-flow climatology is more evident in figure 3.2 which depicts the average value of the observed and simulated discharge for different data sets (E-OBS, REGNIE, EMO-1arcmin, and ERA5-Land) in each month over three decades from 1992 to 2021. The plotted data shows that the observed discharge ranges between 2 and 12 (m^3/s) whereas the maximum value simulated by the model is around 9 (m^3/s). Since the difference between simulated products from different data sets (E-OBS, REGNIE, EMO-1arcmin, and ERA5-Land) is rather small and they are displaying the same pattern a closer look reveals that the model underestimated the discharge for the first three months of the year (January, February, and March), but the prediction is close to the observed values for the next five months (April to August), and the discharge was overestimated for the entire rest of the year (September to December). In other words, the model's performance could have been better during the autumn and winter seasons, but it predicted the discharge more accurately during the spring and summer seasons.

Table 3.1 summarizes the results of the BRNN model for training and testing periods of different data sets in daily time steps. Since the model is fit on the training data, the errors are lower than in the testing period. The model's output, such as Kling-Gupta efficiency (KGE) and root-mean-square error (RMSE), demonstrate that the model performs slightly better on the ERA5-Land data set during both the training and testing periods. The differences between different meteorological products are quite significant, mainly REGNIE and E-OBS in terms of the KGE having the most inferior performance.

3.2 Development And Testing Of NNM Model With LSTM Architecture

The result of the NNM with LSTM architecture for different meteorological inputs such as precipitation and temperature based on E-OBS, REGNIE, EMO-1arcmin, and ERA5-

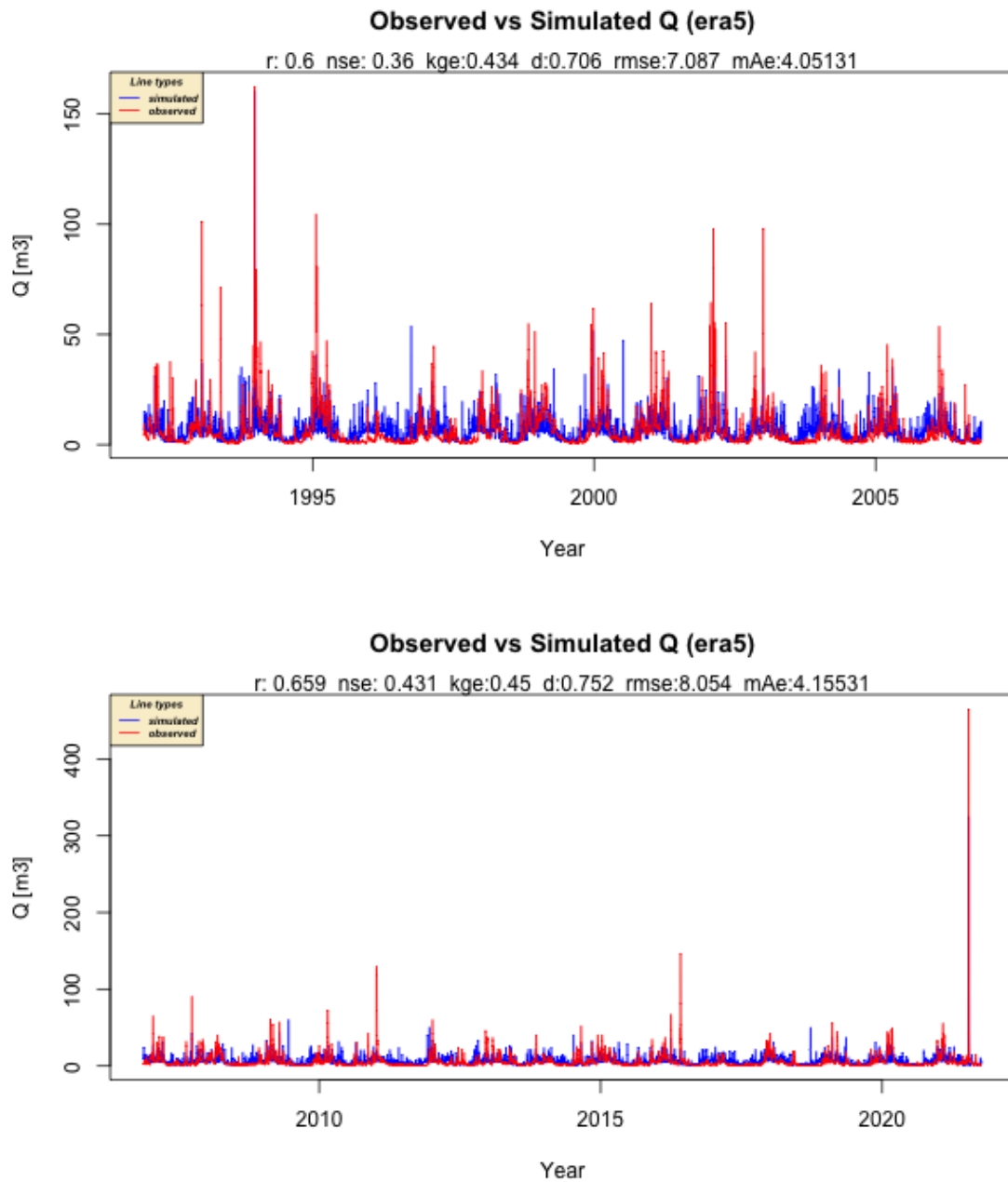


Figure 3.1: Hydro-graph of training (top) and testing (bottom) period by BRNN model for ERA5-Land.

Land in daily time step on the Ahr basin over three decades (1992–2021) is discussed in this part. To operate the model, each simulation was divided into halves to create training and testing periods. The first half or the training period includes data from 1992 to 2007, and the second half or the testing period contains data from 2008 to 2021. The model was

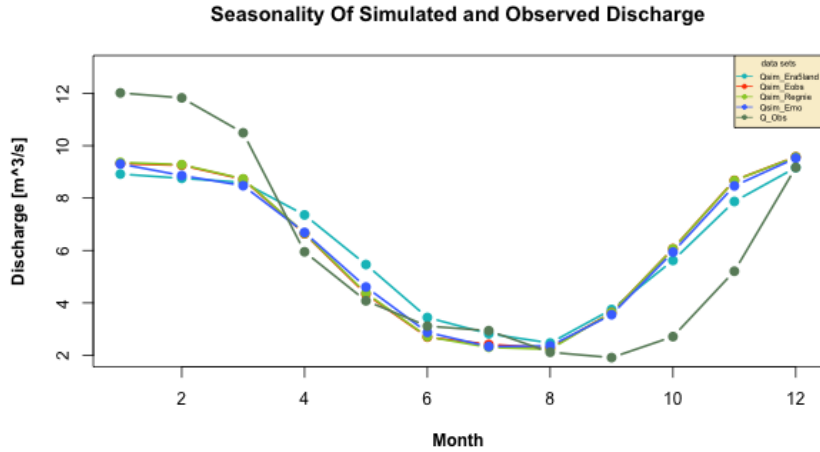


Figure 3.2: The seasonality of simulated discharge by BRNN model based on four data sets (ERA5-Land, EMO-1arcmin, E-OBS, and REGNIE) against observed discharge over 30 years (1992–2021), including both the training and testing periods.

Table 3.1: BRNN results for training and testing periods at daily time steps using precipitation and temperature based on different meteorological data sets (ERA5-Land, EMO-1arcmin, E-OBS, and REGNIE) as input.

Training Period					
data sets	KGE	RMSE	COR	NSE	MAE
ERA5-Land	0.43	7.08	0.6	0.36	4.05
EMO-1arcmin	0.43	7.09	0.59	0.35	3.87
REGNIE	0.21	7.91	0.44	0.2	4.32
E-OBS	0.22	7.9	0.45	0.2	4.31
Testing Period					
ERA5-Land	0.45	8.05	0.65	0.43	4.15
EMO-1arcmin	0.17	9.8	0.4	0.15	3.95
REGNIE	0.1	10.1	0.33	0.1	4.38
E-OBS	0.13	10.1	0.33	0.08	4.4

run based on the mean squared error (MSE) objective function.

Figure 3.3 represents the LSTM model’s implementation during the training and testing phases of an example EMO-1arcmin data set. The MSE was used as the objective function to run the model. The model’s evaluation factors, such as KGE, MAE, and RMSE, indicate that the differences between observed and simulated data (errors) are lower during the training period, whereas testing results in more errors or misclassifications when making predictions. The average value of observed and simulated outflow for various data sets (E-OBS, REGNIE, EMO-1arcmin, and ERA5-Land) in each month over 30 years

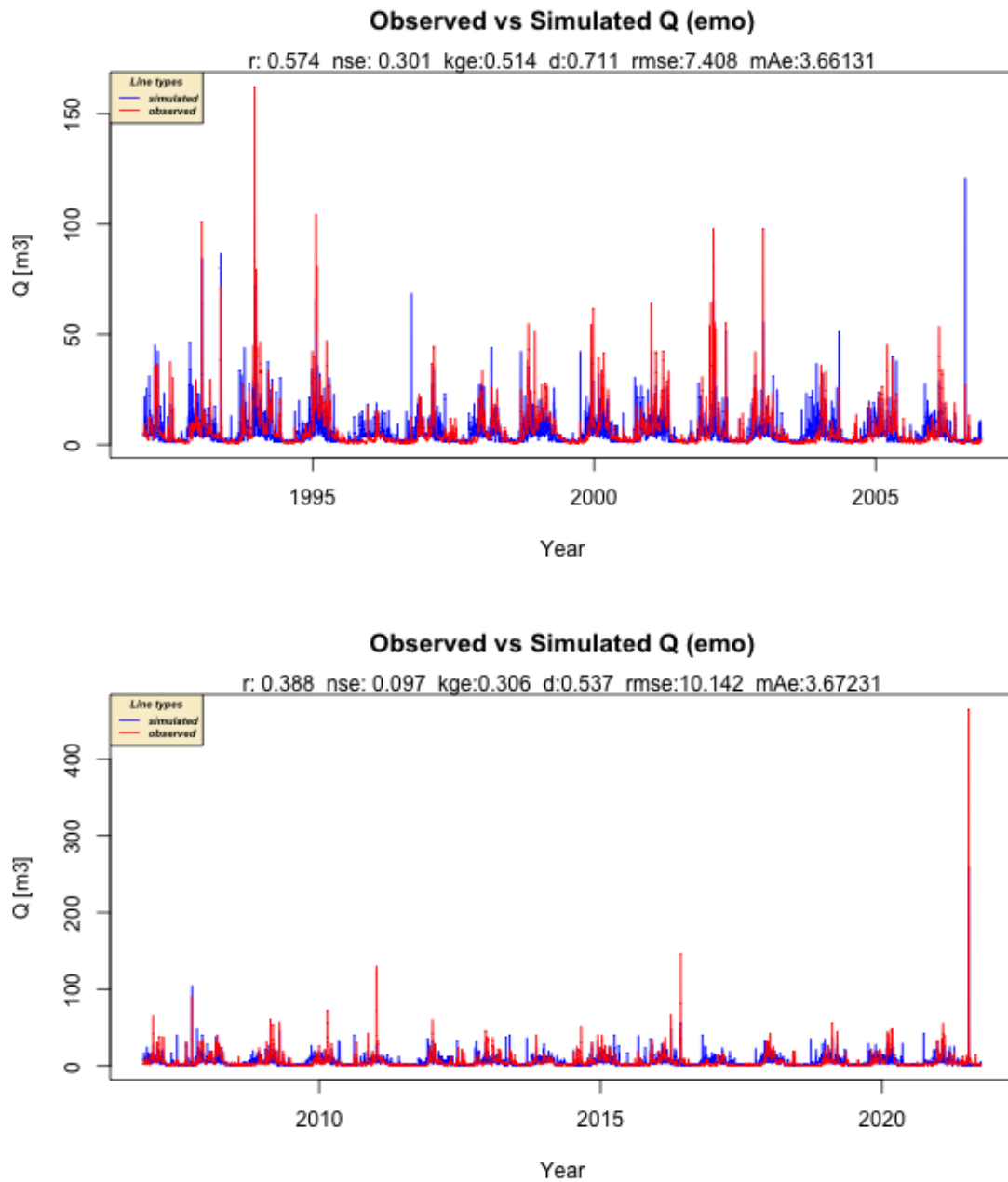


Figure 3.3: Hydrograph at the top: as training and at the bottom: as testing period by LSTM model for EMO-1arcmin.

(1992–2021) derived from the LSTM model shown in figure 3.4 indicates that the mean value of observed discharge is in the range of 2 to 12 (m^3/s), while the model simulates approximately a range of 2 to 8 (m^3/s) for all data sets. Even though all simulated discharges follow the same pattern, the REGNIE and EMO-1arcmin data sets with the ranges

of 2 to 6 (m^3/s) and 2 to 8 (m^3/s) have the lowest and highest accuracy of ranges, respectively. The plotted results in figure 3.4 show that the model underestimated the discharge during the first four months of the year (January, February, March, and April), however, this underestimation decreases during the next four months (May, June, July, and August), and the model at last overestimated the discharge during the rest three months (September, October, and November) and during last month of the year (December) performed with an underestimation. Furthermore, the model performed better during the spring and summer seasons.

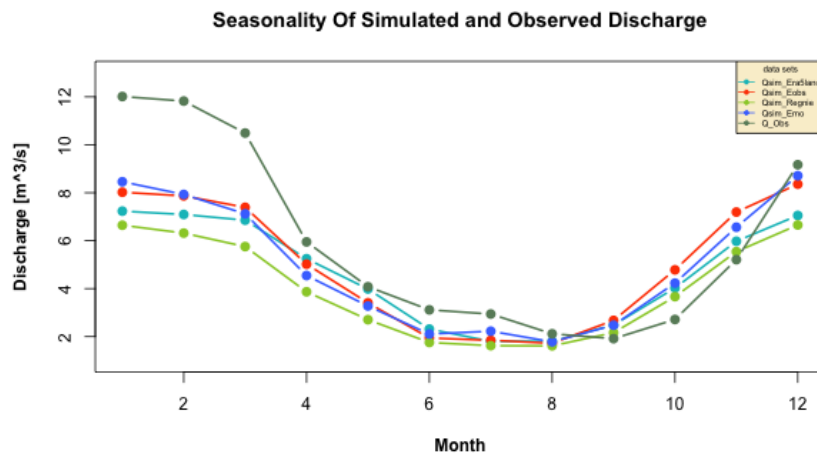


Figure 3.4: The seasonality of simulated discharge by LSTM model using four different data sets (ERA5-Land, EMO-1arcmin, E-OBS, and REGNIE) against observed discharge over 3 decades (1992–2021), including the training and testing periods.

Table 3.2 summarizes the LSTM model’s outcomes for four different data sets’ training and testing periods in daily time scales. The comparison of the results for training and testing periods indicates that the errors are minor during the training period than during the testing period due to the fact that the model is fit on training data. Statistical evaluation factors of the model, such as KGE, RMSE, and MAE results, illustrate that the model function slightly better on the EMO-1arcmin data sets during both the training and testing periods.

Table 3.2: LSTM results for training and testing periods at daily time steps using precipitation and temperature from four different data sets (ERA5-Land, EMO-1arcmin, E-OBS, and REGNIE) as input.

Training Period					
data sets	KEG	RMSE	COR	NSE	MAE
ERA5-Land	0.43	7.19	0.59	0.33	3.82
EMO-1arcmin	0.51	7.40	0.57	0.30	3.66
REGNIE	0.16	8.28	0.44	0.12	3.91
E-OBS	0.25	8.01	0.44	0.18	4.02
Testing Period					
ERA5-Land	0.11	10.0	0.36	0.11	3.74
EMO-1arcmin	0.30	10.1	0.38	0.09	3.67
REGNIE	0	10.3	0.29	0.05	3.75
E-OBS	0.09	10.1	0.31	0.09	4.01

3.3 Development And Testing GR6J Hydrological Model

This section discusses the findings of the GR6J model for meteorological inputs such as precipitation and potential evapotranspiration relying on E-OBS, REGNIE, EMO-1arcmin, and ERA5-Land in a daily time scale on the Ahr watershed over 30 years (1992–2021). Each simulation was segmented into halves to generate calibration and evaluation intervals in order to run the model. The calibration period or the first half spans from 1992 to 2007, and the evaluation period or the second half spans from 2008 to 2021. The model was run based on RMSE objective function.

Figure 3.5 depicts the efficiency of the GR6J model during the REGNIE data set’s calibration (training) and evaluation (testing) periods example. The model was run using the RMSE objective function. KEG and RMSE and MAE values extracted from the model performance point the model’s prediction precision level is higher in the calibration data set than in the evaluation data. However, the model could capture the high signals of discharge during both calibration and evaluation period which is more evident in figure 3.6.

It represents the overall average of the observed and simulated discharge by the GR6J model for four different meteorological inputs (E-OBS, REGNIE, EMO-1arcmin, and ERA5-Land) in each month from 1992 to 2021. The obtained from plotting data shows that the observed discharge ranges from 2 to 12 (m³/s), and the model’s simulated outflows estimate nearly the same range of values and follow the same pattern across all seasons.

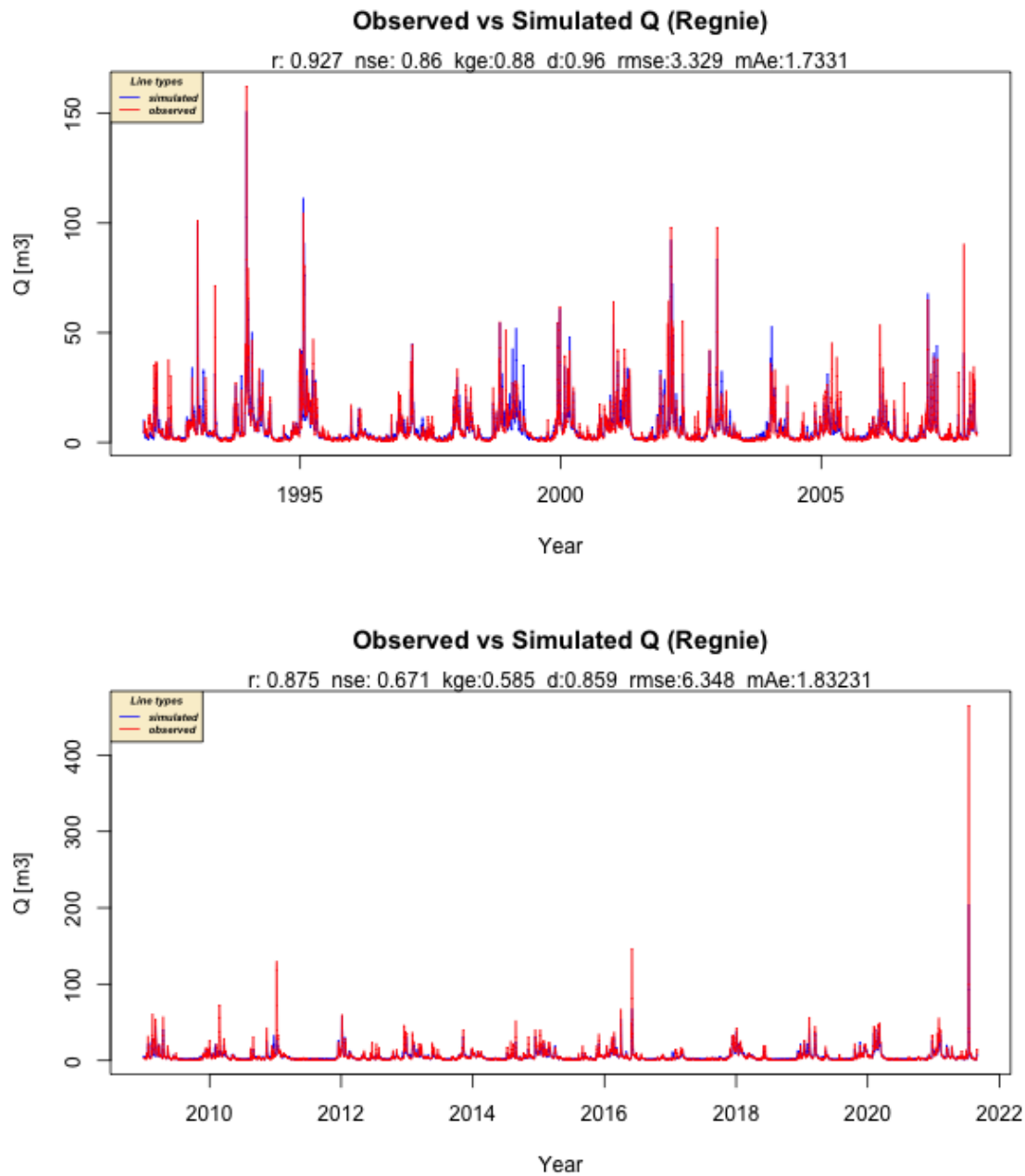


Figure 3.5: Hydro-graph of calibration (top) and evaluation (bottom) period by GR6J model for REGNIE data set.

Table 3.3 outlines the GR6J model’s calibration and evaluation results for four sets of data in daily time frames. The outcomes show the errors are lower during the calibration period. The statistical evaluation factors for the model, such as KGE and RMSE, as well as the MAE findings, demonstrate that the GR6J model performs relatively better on the

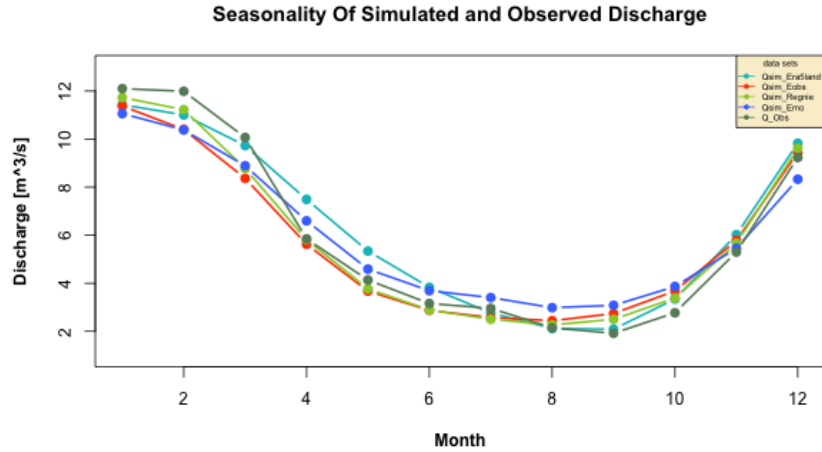


Figure 3.6: The seasonality of simulated discharge by GR6J model based on four meteorological data sets (ERA5-Land, EMO-1arcmin, E-OBS, and REGNIE) against observed discharge over 30 years (1992–2021) including both, the training and testing periods.

REGNIE data sets over the two calibration and evaluation periods. Overall, the results are more satisfactory than the simulations of the BRNN and the LSTM setups. Although the model structure of the GR6J model is fixed and model has only 6 calibration parameters, the model performance is more robust than the flexible model structure of the BRNN and LSTM structures, and it might be possible, that our implementation of these models for simulation daily hydro-graphs is sub-optimal. More research is required to test different configurations of the BRNN and LSTM structures.

Table 3.3: GR6J model results for calibration (training) and evaluation (testing) periods using precipitation and potential evapotranspiration based on four different data sets (ERA5-Land, EMO-1arcmin, E-OBS, and REGNIE) as inputs at daily time steps.

Calibration (training) Period					
data sets	KGE	RMSE	COR	NSE	MAE
ERA5-Land	0.80	4.63	0.85	0.72	2.26
EMO-1arcmin	0.66	5.95	0.74	0.55	2.86
REGNIE	0.87	3.32	0.92	0.85	1.73
E-OBS	0.87	3.55	0.91	0.83	1.90
Evaluation (testing) Period					
ERA5-Land	0.56	6.50	0.82	0.65	2.57
EMO-1arcmin	0.29	9.51	0.51	0.26	2.80
REGNIE	0.58	6.34	0.87	0.67	1.83
E-OBS	0.49	7.22	0.84	0.57	2.05

3.4 Evaluation Of The Modeling Results For The Flood Peak Of July 2021 (As Testing Period)

After evaluating the ability of the three different models to represent daily and seasonal hydro-graphs across different meteorological forcing data, here, we focus on the ability to simulate the floods of July 2021. First, we quantify the cumulative precipitation for four meteorological data sets (ERA5-Land, EMO-1arcmin, E-OBS, and REGNIE) during 2021 as shown in figure 3.7. The rainfall values on the y-axis are in millimeters. Three data sets, E-OBS, REGNIE, and EMO-1arcmin, roughly follow the same pattern and range of values, while ERA5-Land has a positive bias of about 30%, in other words, ERA5-Land significantly overestimates the other three products. The graph shows that all four products exhibit a rapid increase in precipitation during July, which caused the 2021 flood event. During the flood peak, the highest daily recorded amount of precipitation for three meteorological data sets E-OBS, REGNIE, and EMO-1arcmin is around 122 mm.

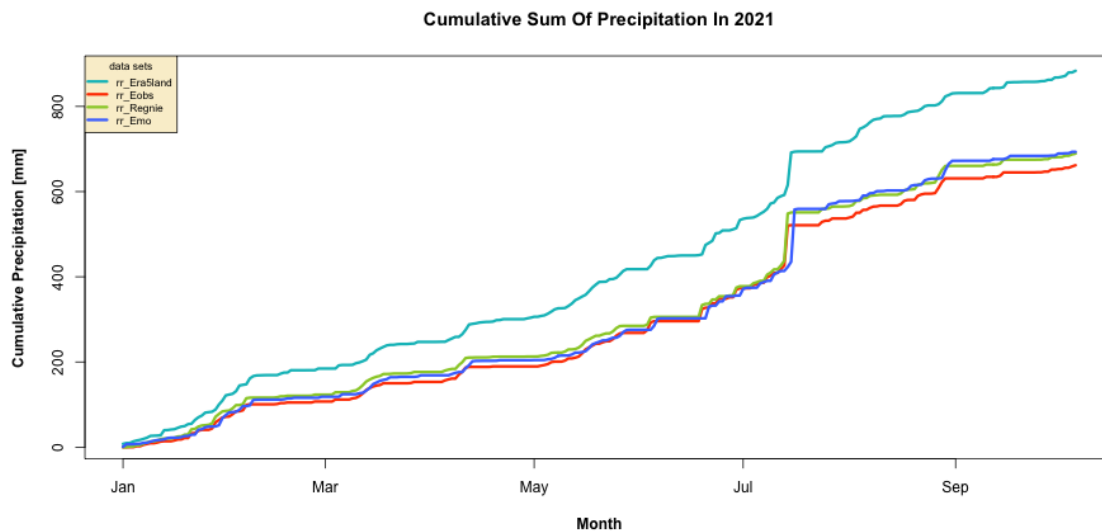


Figure 3.7: The cumulative precipitation based on four meteorological data sets (ERA5-Land, EMO-1arcmin, E-OBS, and REGNIE) in year 2021.

The R-code below shows a simple calculation of cumulative precipitation in R using the base package provided by [R Core Team \(2022\)](#).

```
#required library  
library(base)
```



```
#cumulative precipitation
cumsum(precipitation_data)
```

Furthermore, we evaluate the model simulations based on the parameters obtained during the testing/evaluation period of each model. This means that the model was not trained on the high daily accumulations and extraordinary flood peaks. Table 3.4 shows the observed and simulated discharge by the BRNN model for different data sets for the flood peak of July 14 to 16, 2021 varies very significantly. The results indicate that the simulated discharge by the BRNN model is significantly understated and the model captured the flood signal just for one of the meteorological data sets (ERA5-Land). The best and worst fit of the model to the observed discharge is 325.1784 (m³/s) and 2.101211 (m³/s) from the ERA5-Land and E-OBS data sets, respectively. These results indicate that the model is very sensitive to different meteorological inputs.

Table 3.4: BRNN model results for the flood peak of July 14 to 16, 2021 based on four meteorological data sets (ERA5-Land, EMO-1arcmin, E-OBS, and REGNIE) against observed discharge. All the values are in cubic meters per second (m³/s).

data set	Simulated Q
ERA5-Land	325.1784
EMO-1arcmin	60.837606
REGNIE	2.169170
E-OBS	2.101211
Observed Q	465.3125

For the flood peak of July 14 to 16, 2021, the table 3.5 summarizes the observed and simulated discharge by the LSTM model for various data sets. The findings demonstrate that the LSTM model’s simulated discharge is considerably underestimated as the flood signal is captured just in the EMO-1arcmin data set. The best fit of the model to the observed outflow is 260.120544 (m³/s) from the EMO-1arcmin and the poorest fit is 1.676854 (m³/s) from the REGNIE data sets. Similar to the BRNN setup, also the LSTM model exhibits immense sensitivity to the different meteorological inputs and our LSTM implementation shows very volatile results for changing meteorological inputs, as the other model’s settings remain identical across different setups.

Finally, table 3.6 lists the observed and simulated outflow by the GR6J model for multiple data sets for the flood peak of July 2021. The results show that the model’s

Table 3.5: Results from the LSTM model based on four different data sets (ERA5-Land, EMO-1arcmin, E-OBS, and REGNIE) for the flood peak of July 14 to 16, 2021 against observed discharge. All measurements are in cubic meters per second(m³/s).

data set	Simulated Q
ERA5-Land	5.873678
EMO-1arcmin	260.120544
REGNIE	1.676854
E-OBS	1.800271
Observed Q	465.3125

simulated outflow captured a flood signal for all meteorological inputs from July 14 to 16. The ERA5-Land data set best fits the observed outflow at 271.114514 (m³/s), while the E-OBS data set provides the poorest fit at 144.777877 (m³/s). Despite the fact that the absolute magnitude of the flood peak was not captured, all four meteorological products are capable of displaying an exceptional flood event, which was never simulated in the part. It demonstrates that the hydrological model produces reliable and robust simulations in comparison to the other two data-driven methods.

Table 3.6: The results of the GR6J model based on different meteorological data (ERA5-Land, EMO-1arcmin, E-OBS, and REGNIE) for the flood peak of July 14 to 16, 2021 against observed discharge. All measurements are in cubic meters per second. (m³/s).

data set	Simulated Q
ERA5-Land	271.114514
EMO-1arcmin	231.803866
REGNIE	203.855522
E-OBS	144.777877
Observed Q	465.3125

It is important to note that high-flow events, or floods, are typically associated with the winter and early spring seasons, as shown by climatology hydrographs in Figure 2.6. However, the flood event that transpired during the summer of 2021 was anomalous, happening during a period when water flows are generally low. This anomaly may have contributed to the models' failure to predict the flood's peak accurately. Additionally, the recent study by Kreienkamp et al. (2021) revealed that the floods in Ahr were caused by a high-intensity precipitation event that exceeded the soil's water-holding capacity, resulting in flash floods. This underscores the fact that extreme precipitation is not the sole cause of flooding, as wet soil from previous rainfall may also have played a role in the

floods. These factors are not fully incorporated into models, potentially contributing to the models' failure to anticipate peak flow accurately.

Furthermore, Kreienkamp et al. (2021) noted robust evidence supporting the idea that global warming makes the atmosphere more humid, leading to more intense rainfall. However, other atmospheric and physical processes may alter this relationship. For example, heat release during larger-scale precipitation events may result in even more extreme rainfall events. On more minor scales, atmospheric stability and circulation changes may cause the relationship between humidity and extreme precipitation to be twice as strong as expected. Consequently, rising temperatures may lead to changes in rainfall patterns that make it challenging to detect trends in rare and extreme events like heavy precipitation, making it difficult for models to predict peak flow accurately.

3.5 Evaluation Of The Modeling Results For The Flood Peak Of July 2021 (As Training Period)

To gain a better understanding of the July flood event and the performance of the models, all three types of models (BRNN, LSTM, and GR6J) were calibrated specifically to the year 2021. (i.e., the training/calibration period was set from 01.01.2021 to 30.09.2021) with the available data (precipitation and temperature) from four different data sets (E-OBS, REGNIE, EMO-1arcmin, and ERA5-Land). This is done to test, what the ability of the model would be if all data would be known prior to the model establishment. These outcomes are shown in figure 3.8. It depicts a summary of the calibration results from three different models (BRNN, LSTM, and GR6J) for four different meteorological data sets in 2021. The top four plots show the results of the BRNN model, which could capture the flood peak for ERA5-Land and EMO-1arcmin. The second four plots in the middle show the results of the LSTM model, which also performed perfectly for the ERA5-Land and EMO-1arcmin by capturing the flood apex. The last four plots at the bottom show the GR6J model results, which were satisfactory in estimating flood peaks for all data sets (ERA5-Land, EMO-1arcmin, E-OBS, and REGNIE). The findings of the models in figure 3.8 display that all three models for ERA5-Land and EMO-1arcmin could precisely catch the flood peak, whereas for E-OBS and REGNIE flood apex is captured by the GR6J.

In other words, between data sets, ERA5-Land and EMO-1arcmin had the best model adaptation, and the greatest model performance was for GR6J, which could capture the flood peak for all different data sets (ERA5-Land, EMO-1arcmin, E-OBS, and REGNIE). Overall, the findings are improved, and even if the models for specific meteorological data could not capture the flood peak, they did spot the signals of an outlier. Note that after detailed scrutiny, we discovered that the high-intensity rainfall data from EMO-1arcmin was recorded for one day after the flood event (due to a timing error in the provided netCDF files), so the data based on EMO-1arcmin were shifted back one day to achieve a more accurate result and improve the models' performance.

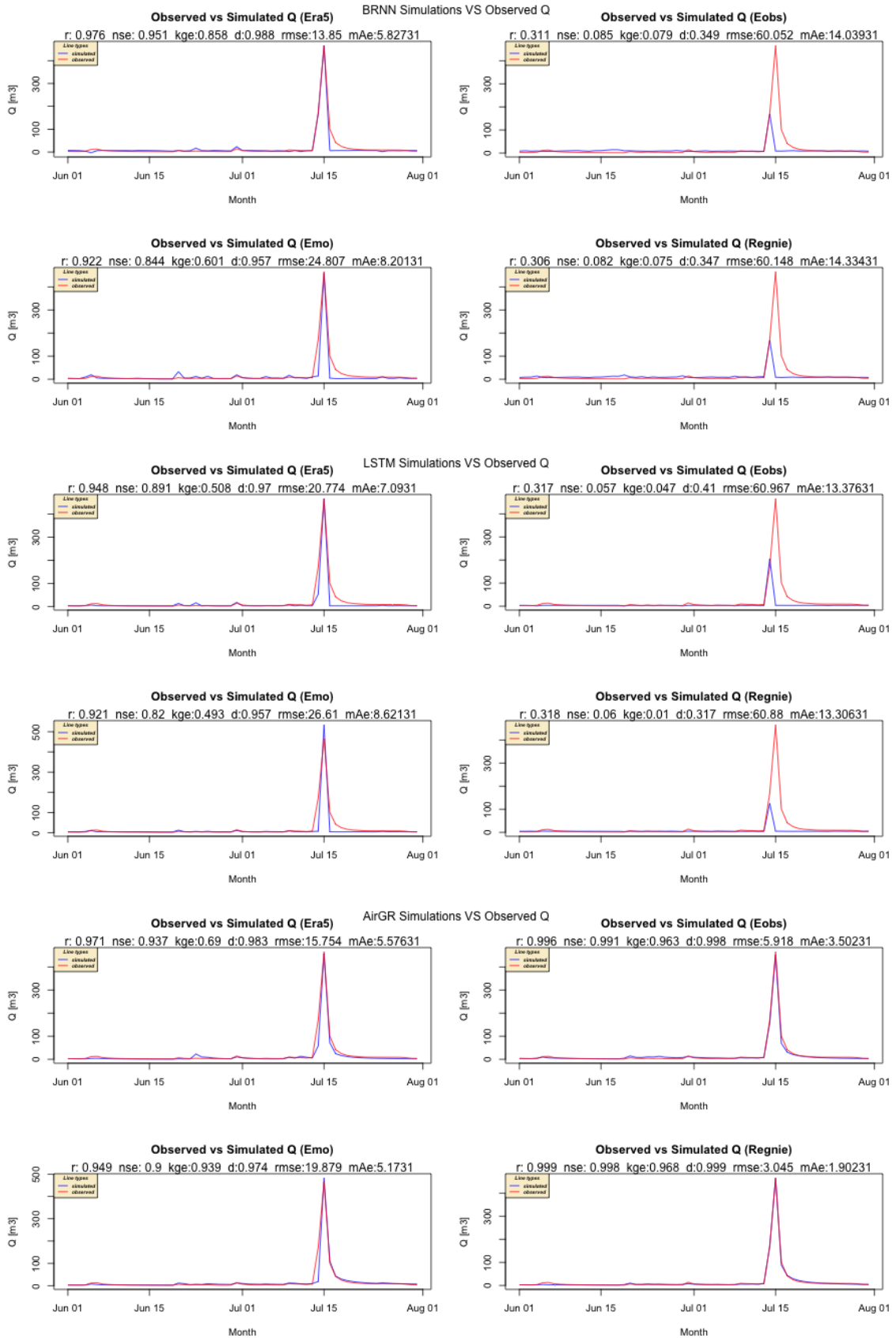


Figure 3.8: Hydro-graph of calibration results for BRNN (top), LSTM (middle), and GR6J (bottom) in 2021 for four meteorological data (ERA5-Land, EMO-1arcmin, E-OBS, and REGNIE).

Chapter 4

Conclusion And Future Work

The events in western Germany in July 2021 called into question our current models' ability to accurately predict the severity of the floods. In this study, hydrological (GR6J) and two data-driven (BRNN and LSTM) models were applied to replicate the daily flows of the Ahr river from 1992 to 2021, taking a variety of input data into account. After validation of the simulated series, this study evaluates the models' performance in estimating the flood peak in July 2021 for the Ahr catchment in Germany. The key findings are as follows:

1. Data-driven models are extremely sensitive to changing meteorological inputs and produce highly unstable results, particularly if they are not trained on high daily accumulations and exceptional flood peaks.
2. Training data-driven models on data with remarkable flood peaks and high daily accumulation values can improve the accuracy of capturing flood signals and, in some cases, the flood peak.
3. In terms of individual values, there is no significant difference between the BRNN- and LSTM-simulated daily runoffs, especially when the models were calibrated to the year 2021 as the training period.
4. Changes in meteorological inputs have little effect on the GR6J model. As a result, it could capture flood signals in all cases, although the maximum flood peak was slightly underestimated in all cases.
5. Training the GR6J with data that included significantly high accumulation values and

a notable flood peak improved the model even further, and as a result, the model was capable of predicting the flood peak for all different input data.

6. The GR6J results outperform the BRNN and LSTM setup simulations. Despite the fact that the GR6J model has a fixed model structure and only six calibration parameters, its performance is more reliable than the BRNN and LSTM models' flexible model structures.

It's worth noting that the BRNN and LSTM models used in our study were built upon models established by [Nasreen et al. \(2022\)](#) where the temporal resolution was annual time scale. However, it is important to recognize that other configurations and hyperparameters may exist that could potentially improve the performance of these models for our task. Nonetheless, because the primary goal of our thesis was to compare the performance of machine learning models with a hydrological model, we did not pursue further research into the BRNN and LSTM model configurations. In the future, it may be worthwhile to investigate additional model architectures and hyperparameters to determine the best configuration for our task.

Another possibility to further enhance this work is to force the hydrological model with the real meteorological forecast, instead of using observation-based data. While the observation-based type of meteorological data was appropriate for our research question and provided us with useful insights into the performance of the models, it is worth considering the potential benefits of using forecasted meteorological data in future research. As a result, it may be worthwhile to run our models with forecasted data in future studies to see if this approach produces better results and quantify the ability of these models to be used for early warning systems. This has the potential to provide new insights into the performance of different models under different conditions, as well as help us refine our understanding of the problem at hand.

Code Availability Statement

The entire source code used in our study is available on the GitHub repository <https://github.com/RonakRah/final-Thesis>, and it can be obtained upon a request via Email: Ronakrahmati25@gmail.com

Bibliography

Abraham, A.: Artificial neural networks, Handbook of measuring system design, 2005.

Allaire, J. and Chollet, F.: keras: R Interface to 'Keras', URL <https://tensorflow.rstudio.com/>, r package version 2.11.0.9000, 2023.

Benton, G., Finzi, M., Izmailov, P., and Wilson, A. G.: Learning invariances in neural networks from training data, Advances in neural information processing systems, 33, 17 605–17 616, 2020.

Bruneo, D. and De Vita, F.: On the use of LSTM networks for predictive maintenance in smart industries, in: 2019 IEEE International Conference on Smart Computing (SmartComp), pp. 241–248, IEEE, 2019.

Campana, D., Comiti, F., Tonon, G., Giammarchi, F., and Kiebacher, T.: Historical channel adjustment in the Ahr river (Italian Alps) and ecological effects of restoration, in: 1st international Conference of Integrative Sciences and sustainable development of rivers, Sommaire, IS Rivers, 2012.

Campana, D., Marchese, E., Theule, J. I., and Comiti, F.: Channel degradation and restoration of an Alpine river and related morphological changes, Geomorphology, 221, 230–241, 2014.

Cornes, R. C., van der Schrier, G., van den Besselaar, E. J., and Jones, P. D.: An ensemble version of the E-OBS temperature and precipitation data sets, Journal of Geophysical Research: Atmospheres, 123, 9391–9409, 2018.

Coron, L., Thirel, G., Delaigue, O., Perrin, C., and Andréassian, V.: The suite of lumped

- GR hydrological models in an R package, *Environmental modelling & software*, 94, 166–171, 2017.
- Coron, L., Perrin, C., Delaigue, O., Thirel, G., Michel, C., Andréassian, V., Bourgin, F., and Brigode, P.: Package ‘airGR’, 2018.
- Coron, L., Delaigue, O., Thirel, G., Dorchie, D., Perrin, C., and Michel, C.: airGR: Suite of GR Hydrological Models for Precipitation-Runoff Modelling, <https://doi.org/10.15454/EX11NA>, URL <https://CRAN.R-project.org/package=airGR>, r package version 1.7.0, 2022.
- Delaigue, O., Thirel, G., Coron, L., and Brigode, P.: airGR and airGRteaching: two open-source tools for rainfall-runoff modeling and teaching hydrology, in: 13th International Conference on Hydroinformatics (HIC 2018), vol. 3, pp. 541–548, Goffredo La Loggia, Gabriele Freni, Valeria Puleo and Mauro De Marchis, 2018.
- Delaigue, O., Thirel, G., Coron, L., and Brigode, P.: airGR and airGRteaching: two packages for rainfall-runoff modeling and teaching hydrology, in: 15th edition of the International R User Conference, p. 1, 2019.
- E-OBS database: E-OBS 2023. https://surfobs.climate.copernicus.eu/dataaccess/access_eobs.php, last access: 20 March 2023, 2023.
- EMO-larcmin database: EMO-larcmin 2023. <https://data.europa.eu/data/data2023>, 2023.
- ERA5-LAND database: ERA5-LAND 2023. <https://cds.climate.copernicus.eu/#!/home>, last access: 20 March 2023, 2023.
- Jain, A. K., Mao, J., and Mohiuddin, K. M.: Artificial neural networks: A tutorial, *Computer*, 29, 31–44, 1996.
- Jeppesen, J.: Fact sheet: Reanalysis, 2021.
- Jokar, M. and Semperlotti, F.: Finite Element Network Analysis: A Machine Learning based Computational Framework for the Simulation of Physical Systems, Accessed: 25 February 2023, https://www.researchgate.net/figure/Expanded-schematic-of-a-bidirectional-recurrent-neural-network-BRNN-showing-its_fig1_343710969, 2020.

- Kakoulaki, G., Gonzalez-Sanchez, R., Gracia Amillo, A., Szabó, S., De Felice, M., Fari-nosi, F., De Felice, L., Bisselink, B., Seliger, R., Kougias, I., et al.: Benefits of Pairing Floating Solar Photovoltaic with Hydropower Reservoirs in Europe (National and Re-gional Level), Available at SSRN 4074448.
- Kaspar, F., Zimmermann, K., and Polte-Rudolf, C.: An overview of the phenological ob-servation network and the phenological database of Germany’s national meteorological service (Deutscher Wetterdienst), *Advances in Science and Research*, 11, 93–99, 2015.
- Kastrati, M. and Biba, M.: A state-of-the-art survey on deep learning methods and appli-cations, *Int. J. Comput. Sci. Inf. Secur.(IJCSIS)*, 19, 53–63, 2021.
- Klein Tank, A., Wijngaard, J., Können, G., Böhm, R., Demarée, G., Gocheva, A., Mileta, M., Pashiardis, S., Hejkrlik, L., Kern-Hansen, C., et al.: Daily dataset of 20th-century surface air temperature and precipitation series for the European Climate Assessment, *International Journal of Climatology: A Journal of the Royal Meteorological Society*, 22, 1441–1453, 2002.
- Klok, E. and Klein Tank, A.: Updated and extended European dataset of daily climate ob-servations, *International Journal of Climatology: A Journal of the Royal Meteorological Society*, 29, 1182–1191, 2009.
- Kreienkamp, F., Philip, S. Y., Tradowsky, J. S., Kew, S. F., Lorenz, P., Arrighi, J., Belle-flamme, A., Bettmann, T., Caluwaerts, S., Chan, S. C., et al.: Rapid attribution of heavy rainfall events leading to the severe flooding in Western Europe during July 2021, *World Weather Attribution*, 2021.
- Kuhn, M.: caret: Classification and Regression Training, URL <https://CRAN.R-project.org/package=caret>, r package version 6.0-93, 2022.
- Kuhn, M., Wing, J., Weston, S., Williams, A., Keefer, C., Engelhardt, A., Cooper, T., Mayer, Z., Kenkel, B., Team, R. C., et al.: Package ‘caret’, *The R Journal*, 223, 2020.
- Legg, S.: IPCC, 2021: Climate change 2021-the physical science basis, *Interaction*, 49, 44–45, 2021.

Maladkar, K.: types of artificial neural networks currently being used in machine learning,” Jan. 2018, 2018.

McLeod, A. I.: Kendall rank correlation and Mann-Kendall trend test, R Package Kendall, 602, 1–10, 2005.

Menne, B., Murray, V., Organization, W. H., et al.: Floods in the WHO European Region: health effects and their prevention, World Health Organization. Regional Office for Europe, 2013.

Mohr, S., Ehret, U., Kunz, M., Ludwig, P., Caldas-Alvarez, A., Daniell, J. E., Ehmele, F., Feldmann, H., Franca, M. J., Gattke, C., Hundhausen, M., Knippertz, P., K pfer, K., M hr, B., Pinto, J. G., Quinting, J., Sch fer, A. M., Scheibel, M., Seidel, F., and Wisotzky, C.: A multi-disciplinary analysis of the exceptional flood event of July 2021 in central Europe. Part 1: Event description and analysis, Natural Hazards and Earth System Sciences Discussions, 2022, 1–44, <https://doi.org/10.5194/nhess-2022-137>, URL <https://nhess.copernicus.org/preprints/nhess-2022-137/>, 2022.

Munich Re: Europe: Extreme flash floods with record losses. <https://www.munichre.com/en/company/media-relations/media-information-and-corporate-news/media-information/2022/natural-disaster-losses-2021.html>, last access: 22 March 2023, 2022.

Mu oz Sabater, J.: First ERA5-Land dataset to be released this spring, ECMWF newsletter, 159, 8–9, 2019.

Mu oz-Sabater, J.: ERA5-Land hourly data from 1950 to 1980, Copernicus Climate Change Service (C3S) Climate Data Store (CDS), 2021.

Nasreen, S., Sou kov , M., Vargas Godoy, M. R., Singh, U., Markonis, Y., Kumar, R., Rakovec, O., and Hanel, M.: A 500-year annual runoff reconstruction for 14 selected European catchments, Earth System Science Data, 14, 4035–4056, 2022.

R Core Team: R: A Language and Environment for Statistical Computing, R Founda-

- tion for Statistical Computing, Vienna, Austria, URL <https://www.R-project.org/>, 2022.
- REGNIE database: REGNIE 2023, last access: 20 March 2023, URL <https://gisc.dwd.de/wisportal/showMetadata.jsp?xml=de.dwd.hydromet.regnie.daily.data>, 2023.
- Rhineland-Palatinate: Altenahr, URL <https://geodaten-wasser.rlp-umwelt.de/wasserstand/2718040300/stammdaten>, 2021.
- Roggenkamp, T. and Herget, J.: Reconstructing peak discharges of historic floods of the River Ahr, Germany, *Erdkunde*, pp. 49–59, 2014.
- Ryan, T.: LSTMs explained: A complete, technically accurate, conceptual guide with keras, 2021.
- Saadi, M., Furusho-Percot, C., Belleflamme, A., Chen, J.-Y., Trömel, S., and Kollet, S.: How uncertain are precipitation and peak flow estimates for the July 2021 flooding event?, *Natural Hazards and Earth System Sciences*, 23, 159–177, 2023.
- Saxena, S.: Introduction to Long Short Term Memory (LSTM) , Accessed: 25 February 2023, <https://www.analyticsvidhya.com/blog/2021/03/introduction-to-long-short-term-memory- lstm/>, 2021.
- Schulzweida, U., Kornblueh, L., and Quast, R.: CDO user guide, Climate data operators, Version, 1, 205–209, 2006.
- Siarni-Namini, S., Tavakoli, N., and Namin, A. S.: The performance of LSTM and BiLSTM in forecasting time series, in: 2019 IEEE International Conference on Big Data (Big Data), pp. 3285–3292, IEEE, 2019.
- Singh, A.: Artificial Neural Network — Types — Feed Forward — Feedback — Structure — Perceptron — Machine Learning — Applications , Accessed: 25 February 2023, <https://msatechnosoft.in/blog/artificial-neural-network-types-feed-forward-feedback-structure-perceptron-machine-learning-applications/>, 2018.

- Szymczak, S., Backendorf, F., Bott, F., Fricke, K., Junghänel, T., and Walawender, E.: Impacts of Heavy and Persistent Precipitation on Railroad Infrastructure in July 2021: A Case Study from the Ahr Valley, Rhineland-Palatinate, Germany, *Atmosphere*, 13, 1118, <https://doi.org/10.3390/atmos13071118>, URL <http://dx.doi.org/10.3390/atmos13071118>, 2022.
- Thiemig, V., Gomes, G. N., Skøien, J. O., Ziese, M., Rauthe-Schöch, A., Rustemeier, E., Rehfeldt, K., Walawender, J. P., Kolbe, C., Pichon, D., et al.: EMO-5: a high-resolution multi-variable gridded meteorological dataset for Europe, *Earth System Science Data*, 14, 3249–3272, 2022.
- Truedinger, A. J., Jamshed, A., Sauter, H., and Birkmann, J.: Adaptation after Extreme Flooding Events: Moving or Staying? The Case of the Ahr Valley in Germany, *Sustainability*, 15, 1407, 2023.
- U.S. Geological Survey: Global Multi-resolution Terrain Elevation Data 2010 (GMTED 2010), URL <https://www.usgs.gov/centers/eros/science/usgs-eros-archive-digital-elevation-global-multi-resolution-terrain-elevation>, last accessed on 2020-03-09, 2018.
- Wang, Q., Hapuarachchi, H., and Pagano, T.: A review of advances in flash flood forecasting available at [http, onlinelibrary. wiley. com/doi/10.1002/for](http://onlinelibrary.wiley.com/doi/10.1002/for), 1210, 2771–2784, 2011.
- Ye, Y., Jiao, W., and Yan, H.: Managing relief inventories responding to natural disasters: Gaps between practice and literature, *Production and Operations Management*, 29, 807–832, 2020.
- Zou, J., Han, Y., and So, S.-S.: Overview of artificial neural networks, *Artificial neural networks: methods and applications*, pp. 14–22, 2009.